NIST Technical Note 1771

A Study of Thermal Behavior of a Composite Floor System in Standard Fire Resistance Tests

Dilip Banerjee

http://dx.doi.org/10.6028/NIST.TN.1771

National Institute of
Standards and Technology
U.S. Department of Commerce

NIST Technical Note 1771

A Study of Thermal Behavior of a Composite Floor System in Standard Fire Resistance Tests

Dilip Banerjee
Materials and Structural Systems Division
Engineering Laboratory

http://dx.doi.org/10.6028/NIST.TN.1771

October 2012

U.S. Department of Commerce
Rebecca Blank, Acting Secretary

National Institute of Standards and Technology
Patrick D. Gallagher, Under Secretary of Commerce for Standards and Technology and Director

Certain commercial entities, equipment, or materials may be identified in this document in order to describe an experimental procedure or concept adequately. Such identification is not intended to imply recommendation or endorsement by the National Institute of Standards and Technology, nor is it intended to imply that the entities, materials, or equipment are necessarily the best available for the purpose.

National Institute of Standards and Technology Technical Note 1771
Natl. Inst. Stand. Technol. Tech. Note 1771, 46 pages (October 2012)
http://dx.doi.org/10.6028/NIST.TN.1771
CODEN: NTNOEF

Table of Contents

Abstract 5
1 Introduction 6
2 Description of the Fire Resistance Tests 6
  2.1 Test Specimen 7
  2.2 Furnace 8
  2.3 Instrumentation 9
  2.4 Test Procedure 10
3 Experimental Results 11
  3.1 General Observations of Tests 11
  3.2 Furnace Thermal Environment 11
  3.3 Unexposed Concrete Slab Surface Temperatures 13
  3.4 Steel Temperatures 14
  3.5 Variability in Experimentally Recorded Temperatures 16
4 Heat Transfer Modeling 20
  4.1 Methodology 20
  4.2 Thermophysical Properties, Boundary and Initial Conditions 22
  4.3 Interpolation of Temperatures 23
5 Evaluation of the Heat Transfer Model 24
  5.1 Test 1 24
  5.2 Test 2 27
  5.3 Effect of SFRM Dislodgement 32
6 Summary 34
7 References 36
8 Acknowledgment 37
Appendix A: Thermophysical properties 38
  1. Steel 38
  2. Concrete 40
  3. SFRM 41
Appendix B: Finite Element Model of the Composite Floor System 43
Appendix C: Log of Observations in Test 1 45
Appendix D: Log of Observations in Test 2 46

Abstract

The National Institute of Standards and Technology (NIST) conducted a series of four standard fire resistance tests of the composite floor system used in the World Trade Center (WTC) towers. These tests were conducted as part of NIST's investigation into the collapse of the WTC towers. The main objectives of these tests were to understand the effects of three key factors on the fire behavior of composite floor systems during fire exposure. These factors were: a) thickness of fireproofing on steel, b) test restraint conditions, and c) scale of the test (e.g., full scale vs. reduced scale). Two tests were conducted using full-scale test specimens while two other tests were conducted using reduced-scale test specimens. In this report, only the results from the two full-scale tests are discussed and compared against numerical predictions. These two thermally-similar fire resistance tests were conducted by the Underwriters Laboratories (UL) of Canada by exposing a composite floor system to the heating profile (time-temperature curve) specified in the ASTM E119 standard. In these tests, the fire environment was well controlled and measured. Also, the temperature and deflection data were recorded at sufficient number of locations to characterize the structural performance of the test assemblies over time. Since a large set of well controlled measurements (both thermal and structural) are available, data from these tests were used for development and evaluation of numerical models to understand the thermal and structural behavior of composite floor systems during fire exposure.

This report summarizes the characterization of the furnace thermal environment and thermal behavior of members during the fire tests. Additionally, numerical results from a heat transfer finite element model of a representative section of the floor system are compared against data obtained in the full-scale tests to evaluate the finite element heat transfer model. Future work will focus on determining uncertainties in predicting temperatures of structural members using experimental data collected during NIST's WTC fire resistance tests.

1 Introduction

Predicting structural behavior under fire requires an accurate modeling of (a) thermal environment in a fire, (b) heating of structural elements exposed to hot gases from fire, and (c) structural response to both thermal and gravity loads. There are uncertainties associated with the computed results in each of these steps, which propagate from one step to the next. In analyzing uncertainty propagation, the goal is to determine how random variation, lack of knowledge, or error affects the sensitivity, performance, or reliability of the system that is being modeled. The predicted results need to provide time-dependent temperatures in structural members during a fire event, along with the associated uncertainties.

A comparison of numerical predictions of the temperature field against carefully controlled fire resistance experiments can provide insight into the uncertainties associated with prediction of the temperature histories of structural elements exposed to fire. However, data from such well controlled full-scale fire resistance tests are difficult to obtain from the literature. Since a rich set of data from the National Institute of Standards and Technology (NIST)'s fire resistance tests of composite floor systems is available, validation efforts have been focused on these tests. Toward this end, a finite element heat transfer model of the composite floor truss section was constructed in ANSYS [1] to model the heating profile of the structural members exposed to the standard fire.

Although the details of each fire resistance test are described in ref. [2], a brief summary of the thermal behavior of steel members and characterization of the furnace environment are provided here. In this report, the experimental set up and the fire resistance tests are described first. Then experimental results collected at several locations in the trusses and furnace are presented. A brief statistical analysis of member temperatures measured during the full-scale tests is then provided. Finally, numerical results from the heat transfer model are compared against experimental data. A quantitative estimate of the agreement between the experimental and simulation results is then provided. Future work will focus on estimating uncertainties in member temperatures.

2 Description of the Fire Resistance Tests

As part of its investigation into the collapse of the World Trade Center (WTC) towers, NIST conducted four fire resistance tests of composite floor systems (two full-scale and two reduced-scale). These tests were carried out by Underwriters Laboratories (UL) by subjecting composite floor systems to the heating profile (time-temperature curve) specified in the ASTM E-119 standard in a test furnace.

The tests were conducted in both restrained and unrestrained condition to study the performance of the floor systems under the standard fire exposure. Note that in a restrained test, thermal expansion at the supports of a load carrying element due to

exposure to elevated temperatures in fire is resisted by forces external to the element. On the other hand, an element is free to expand and rotate at its supports in an unrestrained test. In this section, a brief description is provided about the test specimens, test furnace, instrumentation, and test procedure pertaining to the two full-scale tests.

2.1 Test Specimen

The floor system for the WTC towers consisted of a lightweight concrete floor slab acting compositely with steel trusses bridging between the building's core columns and exterior wall columns. The main composite trusses, which were used in pairs, spanned either 60 ft.[1] (18.3 m) or 35 ft. (10.7 m) Steel double angles formed the top and bottom chords of the trusses while round bars were used for the web diagonals. Additionally, the floor system included bridging trusses perpendicular to the main trusses.

Passive fire protection was provided by spray applied fire resistive material (SFRM), commonly referred to as "fireproofing," applied directly to the steel members of the trusses. Fireproofing thickness was specified to be 0.75 in. (19 mm). Figure 1(a) shows a cut-away of the floor system illustrating the main trusses, bridging trusses, metal deck, and concrete floor slab used in the WTC towers. Figure 1(b) shows a cross-sectional view of the basic configuration of the truss floor system.

Trusses used in the WTC towers were fabricated from ASTM A242 grade steel [2]. Since this steel was no longer available, ASTM A572 Grade 50 steel was found to be an acceptable substitute by NIST based on a comparison of thermal and mechanical properties of both steels. For the full-scale fire resistance tests, ASTM A572 Grade 50 steel test specimens were constructed to model the 35 ft. (10.7 m) span floor trusses. The deck consisted of 1½ in. (38.1 mm). deep 22 gauge galvanized sheet metal floor units. Compressive strength of the concrete floor slab was specified to be 3000 psi (20.7 MPa). The sprayed fire resistive material used on the test assemblies was BLAZE-SHIELD Type DC/F, which is manufactured by Isolatek International. The SFRM was applied to a thickness of ¾ in. (19 mm). with close tolerances of approximately ±1/16 in. (1.6 mm). The test specimen comprised two main trusses, two bridging trusses, and a floor deck (Figure 2).

Two full-scale standard fire resistance tests were conducted at the Underwriters laboratories fire testing facilities:

1. Test 1: restrained test condition.
2. Test 2: unrestrained test condition.

[1] The policy of NIST is to use the International System of Units (metric units) in all publications. In this document, however, units are presented in metric units or the inch-pound system, whichever is prevalent in the discipline.

2.2 Furnace

The Underwriters Laboratories of Canada (ULC) fire testing facility in Toronto, Canada was used for the fire resistance tests. ULC has a furnace with nominal dimensions of 35 ft. (10.7 m) by 14 ft. (4.3 m). The inside furnace depth is approximately 5 ft. (1.5 m) Test assemblies were constructed so that the top of the floor assembly was nearly flush with the top of the reaction frame. The combustion system consisted of 80 individual floor mounted burners, arranged in an evenly spaced grid of 8 rows with 10 burners in each row for producing furnace temperatures that are as uniform as possible.

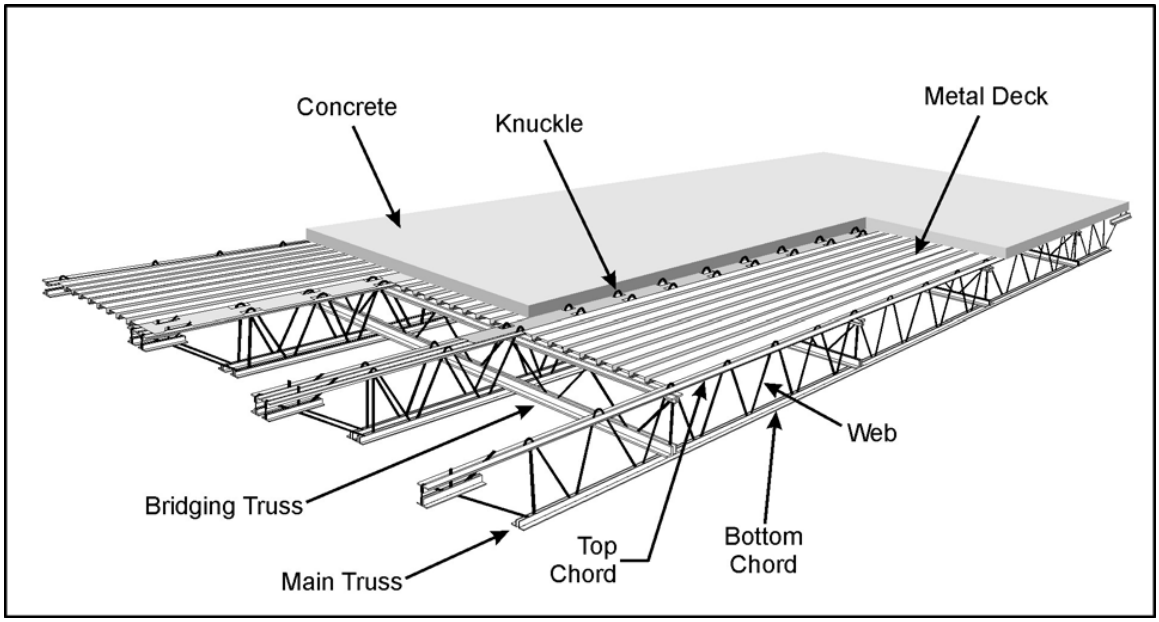

Figure 1(a). Floor system of the WTC towers [3].

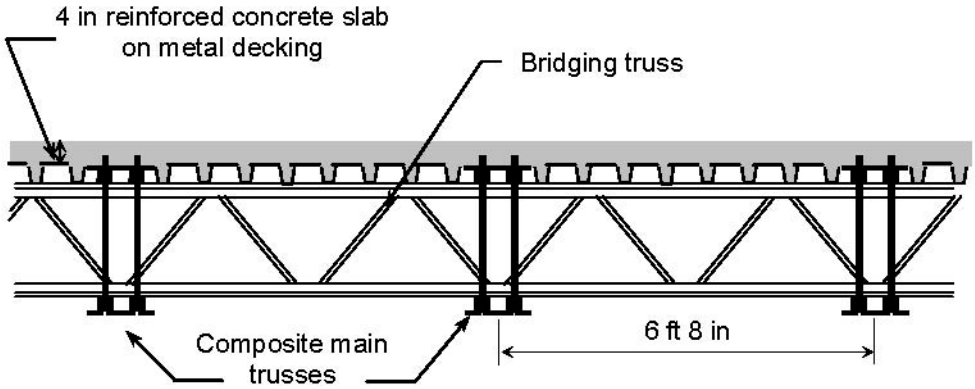

Figure 1(b). Schematic of floor system viewed along the main steel trusses (not to scale) [3].

2.3 Instrumentation

The furnace temperature was measured by means of 24, 16-gauge, Type K thermocouples, sheathed in Inconel pipe symmetrically located in the furnace chamber, as required by the ASTM E-119 standard. The thermocouples were positioned about a foot below the bottom surface of the exposed floor slab. In addition to the furnace thermocouples, Wickstrom plate thermocouples and aspirated thermocouples were also used to monitor furnace temperatures. In addition, heat flux gauges were also used to characterize the thermal environment inside the furnace.

A total of 88 thermocouples were used to measure steel temperatures at various locations along the trusses [2]. Figure 2 shows thermocouple locations in the main trusses. Instrumentation was also added to measure temperature on the unexposed surface of the concrete slab at several locations [2].

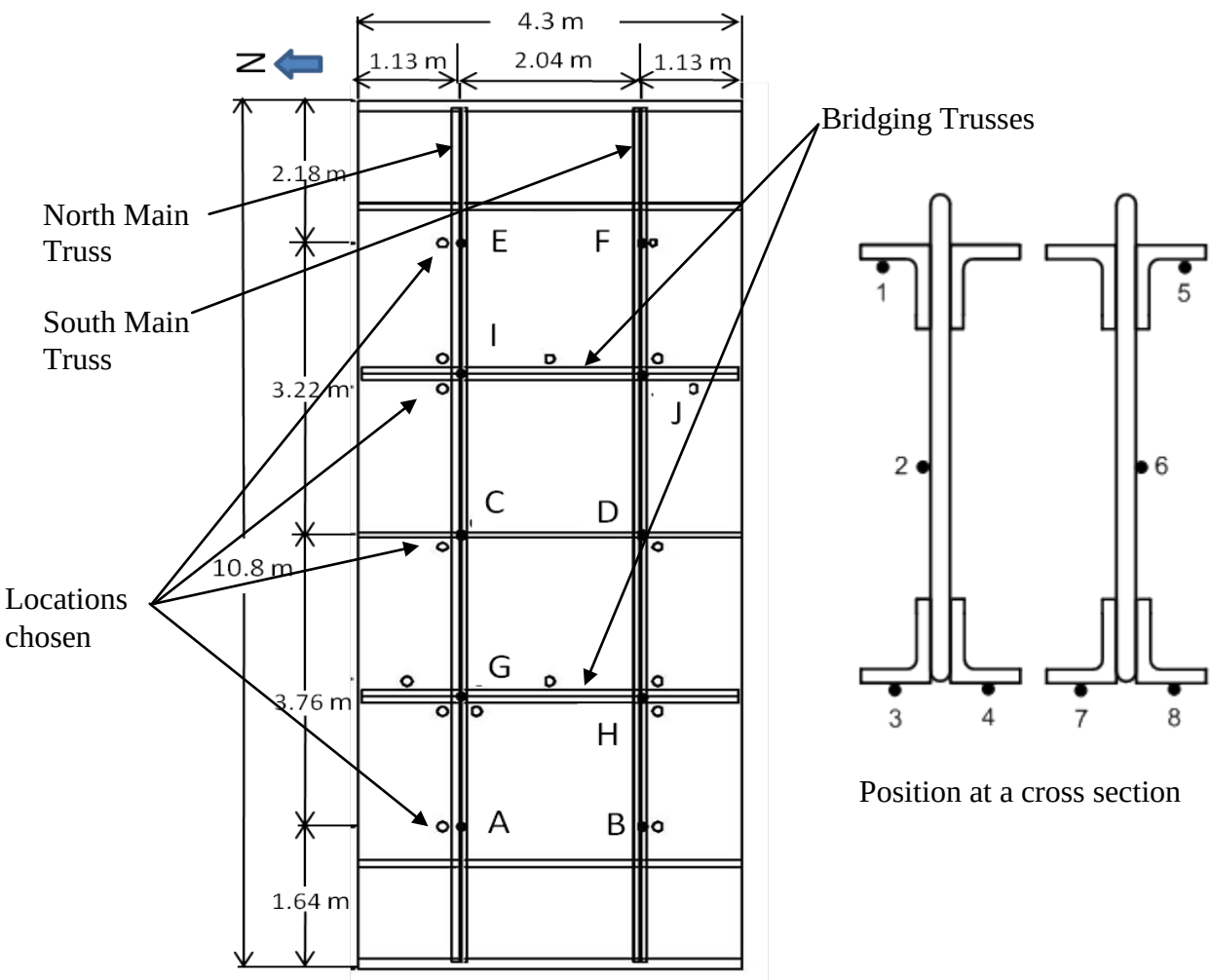

Figure 2: Thermocouple locations in the main truss in the UL tests [1].

2.4 Test Procedure

The tests were conducted according to the procedure specified in the ASTM E119 standard [4]. The ASTM E119 standard prescribes a standard fire exposure for comparing the test results of building construction assemblies. For the tests of floors and roofs, the full design load is applied to the specimen and the standard fire exposure is applied to the underside of the specimen. The assembly is evaluated for its ability to contain the fire by limiting flame spread and by limiting heating of the unexposed surface while maintaining the applied load. Acceptance criteria are provided in terms of time to reach the stipulated average and maximum temperatures both on the unexposed surface and in steel members. The assembly is given a rating, expressed in hours, based on these acceptance, or endpoint, criteria.

The average of 24 thermocouple readings of furnace temperatures for both tests is shown in Figure 3. Also shown is the prescribed ASTM E119 curve. Although there are fluctuations in temperatures recorded by the furnace thermocouples especially during the initial periods of the test, the mean temperatures seem to follow the ASTM E119 curve very well. Note that the furnace temperatures for Tests 3 and 4 are also shown but are not discussed in this report.

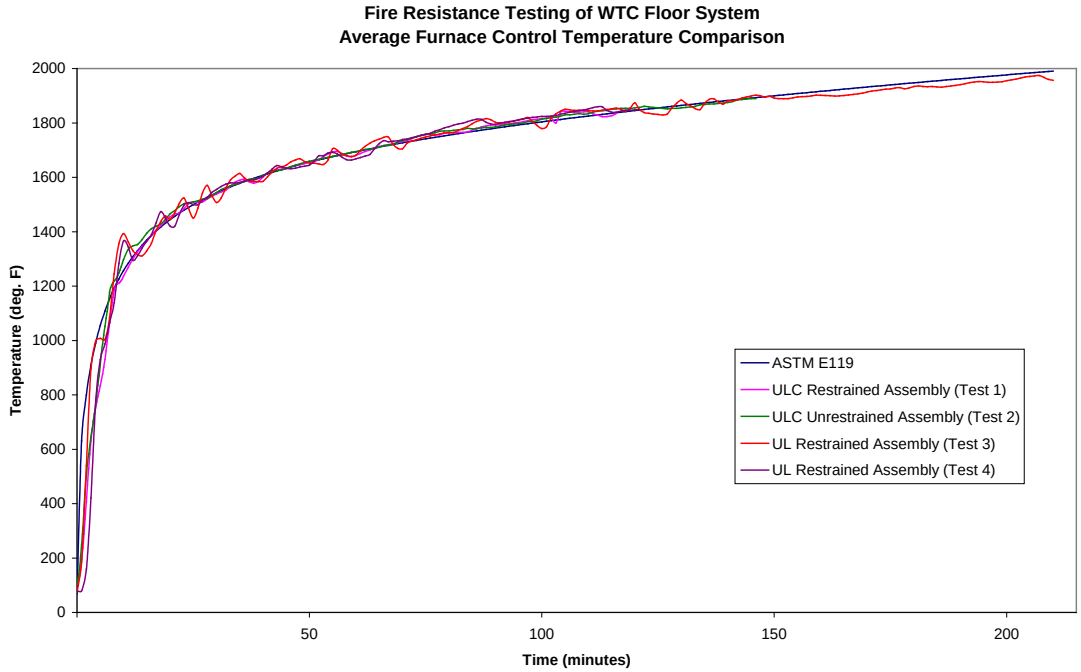

Figure 3: Average furnace temperatures and the specified ASTM E119 curve [1].

The details of the test assembly preparation as well as the loading procedure are described in detail in Ref. [2].

3 Experimental Results

3.1 General Observations of Tests

In Test 1, loud noises (described as “reports” in [2]) were heard beginning roughly fifteen minutes after the start of the test (see Appendix C for a log of observations throughout these tests). These loud reports continued and were often accompanied by noticeable bulging of the metal deck and the dislodging of deck fireproofing. It is believed that these loud noises were associated with spalling of the concrete on the underside of the slab.

Reports were also heard during Test 2, of the 35 ft. (10.7 m) unrestrained specimen, but were not as loud as those observed during Test 1. Post-test inspection of the top of the concrete slab showed very little cracking. Since there was a gap between the concrete slab and the test frame, thermal expansion of the slab did not produce a state of stress that resulted in significant and sudden cracking and crushing similar to this test. Appendix C and D provides a log of the reports observed during the tests.

3.2 Furnace Thermal Environment

In addition to the 24 sheathed thermocouples that were used to measure and monitor furnace temperatures, furnace temperatures were also measured with plate and aspirated thermocouples. Plate thermocouples are used to measure gas temperatures with a surface similar in terms of emissivity, size, and orientation to the specimen surface. Aspirated thermocouples help decrease the magnitude of error by reducing the radiative exchange between the thermocouple and its surroundings. In fact, temperatures measured by aspirated thermocouples are closer to the true gas temperatures [5].

Figures 4 and 5 show the temperatures measured by plate and aspirated thermocouples respectively. It is evident from these figures that the thermal environment in these two tests was similar.

Since thermal radiation is the dominant form of heat transfer, especially at elevated temperatures, heat flux measurements provide a better indication of how quickly a specimen will heat than gas temperatures. For Test 2, radiometer readings were not available, due to damage to the radiometers. For Test 1, the radiative heat flux was about 60 kW/m^2 at the end of 104 minutes, after which the heat flux data showed wide fluctuation and data became unreliable (Figure 6). A dip in the curve at about 50 minutes into the test indicates that the probes recorded a lower radiative heat flux. A change in “view factors” resulting possibly from concrete spalling around that time could have contributed to a lower value of heat flux recorded (see the log of the test in Appendix C).

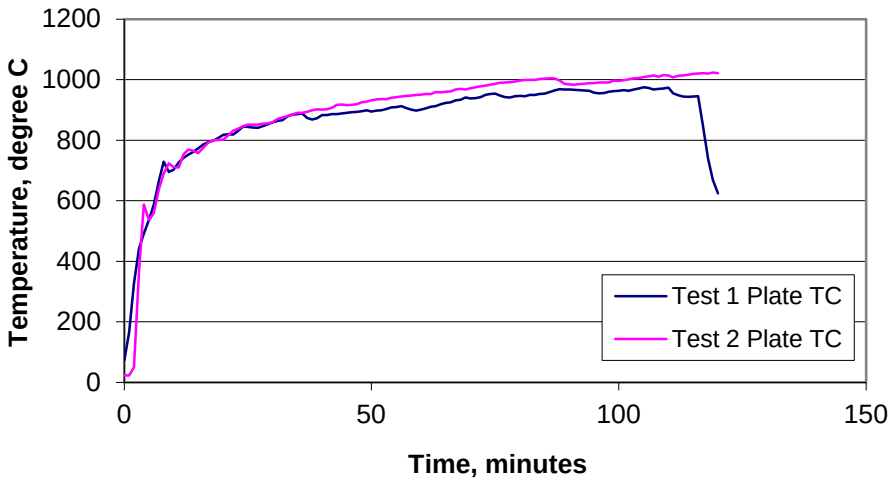

Figure 4: Temperatures measured by plate thermocouples in tests 1 and 2 [2].

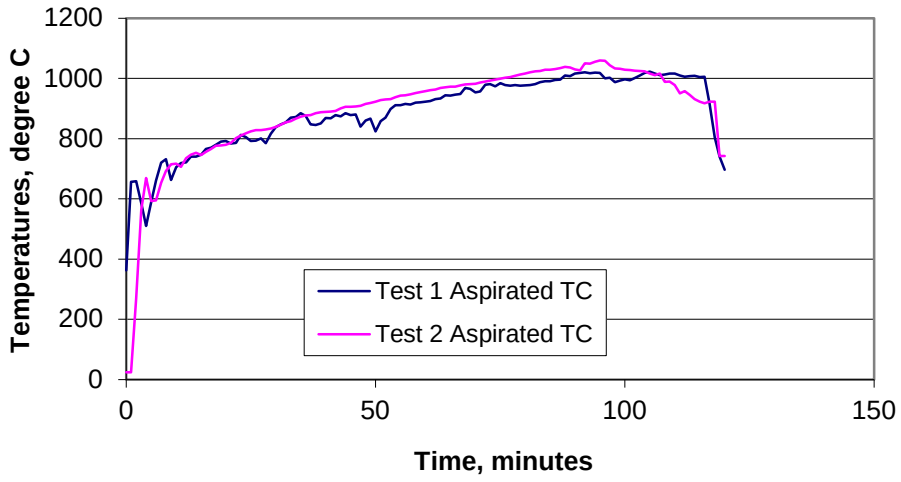

Figure 5: Temperatures measured by aspirated thermocouples in tests 1 and 2 [2].

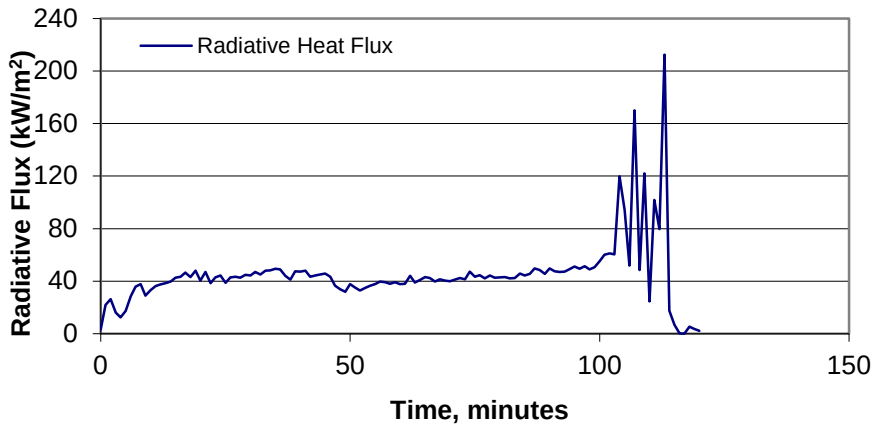

Figure 6: Radiative heat flux in Test 1 [2].

3.3 Unexposed Concrete Slab Surface Temperatures

The average temperature of the top (unexposed) surface of the floor assemblies is plotted in Figure 7. It is observed that the unexposed surface temperatures of both test assemblies were similar prior to the onset of significant concrete crushing and spalling at around 50 minutes in Test 1. Thereafter, the average unexposed surface temperature in Test 1 steadily increased in comparison to that in Test 2 as shown in Figure 7. Two factors could have contributed to higher unexposed surface temperatures in Test 1: a) Spalling of concrete slab at several locations thereby offering less resistance to heat flow through the slab and b) effect of varying moisture level on concrete thermal conductivities.

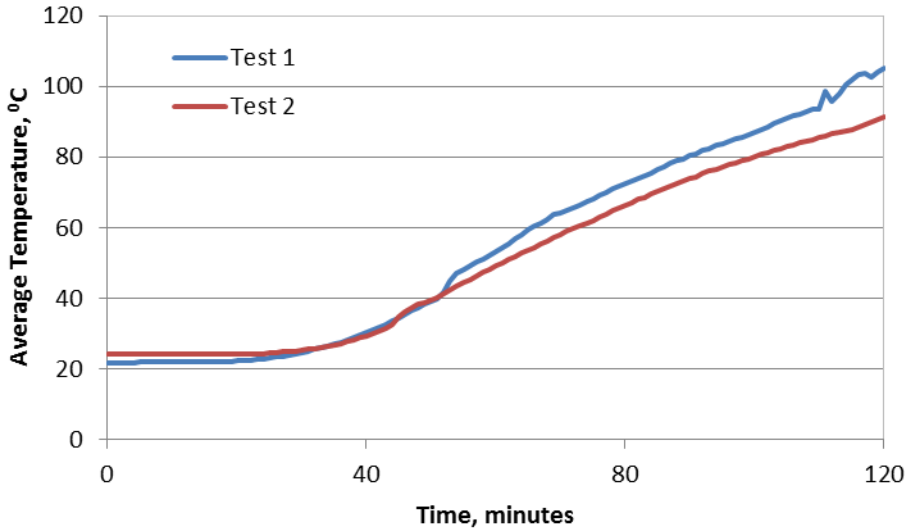

Figure 7: Average concrete slab temperature on unexposed surface in Tests 1 and 2.

3.4 Steel Temperatures

Figures 8(a) through 8(d) show a comparison of average temperatures at the bottom chord for both tests at four locations e.g., A, C, I, and E (refer to Figure 2 for thermocouple locations). For the bottom chords, there were four thermocouples (two on each angle at the bottom chord). Figure 8 shows average temperatures at each angle in the bottom chord (as measured by TC 3 & 4 and TC 7 & 8 respectively). These plots show that the heating trends in the bottom chords are similar in both tests, until about 60 minutes into the test when data from Test 1 showed an abrupt increase in recorded temperatures, possibly due to dislodgement of SFRM as a result of concrete spalling (Figure 8(d)). However, the plots also show a wide variability in temperatures recorded by thermocouples on two angles at the bottom chord (e.g., Fig. 8(a): "Test 1, Section A, TC 3 & 4", and "Test 1, Section A, TC 7 & 8").

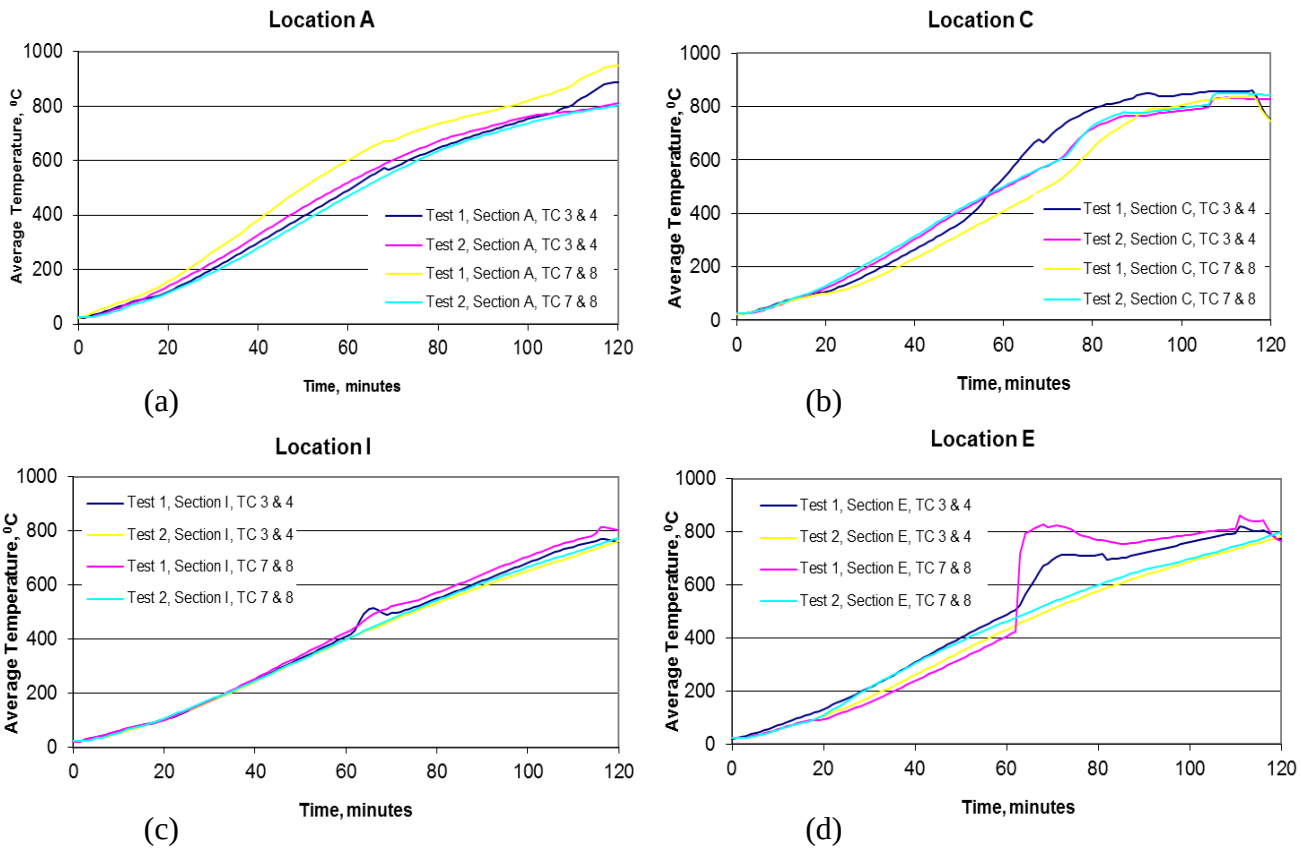

Figure 8 (a) through (d): Comparison of two average temperatures in the bottom chord in Test 1 and 2 [2].

Figures 9 (a) through (d) show a comparison of average temperatures recorded by the thermocouples at the top chord of both the test specimen. Individual thermocouple temperatures have been shown when data for both the thermocouples at the top chord were not available for a particular location along the main truss. It is possible that dislodgement of SFRM took place at around 60 minutes in Test 1 near locations I, C, and E. For Test 2, it appears that such possible dislodgement took place in the vicinity of location C at about 70 minutes into the test. Heating trends for both the tests were generally similar. Location E shows the most discrepancy in measured temperatures between Test 1 and 2 after about 60 minutes into the test.

Most thermocouples at the top chord recorded maximum temperatures of less than 400 ˚C after 2 hours of heating in both the tests. Some thermocouples recorded abrupt temperature increases, possibly due to the dislodgement of SFRM. A quantitative comparison between thermal results in the two tests is provided later in this section.

Figures 10(a) through (d) show a comparison of average temperatures in the two tests for four locations at mid-web along a main truss. Although time-dependent temperatures at location A for both the tests were close to each other (until about 100 minutes into the test for Test 1 when thermocouple data became unreliable and showed wide fluctuations in temperatures), the average temperatures in Test 1 were higher than those in Test 2 for locations C, I, and E.

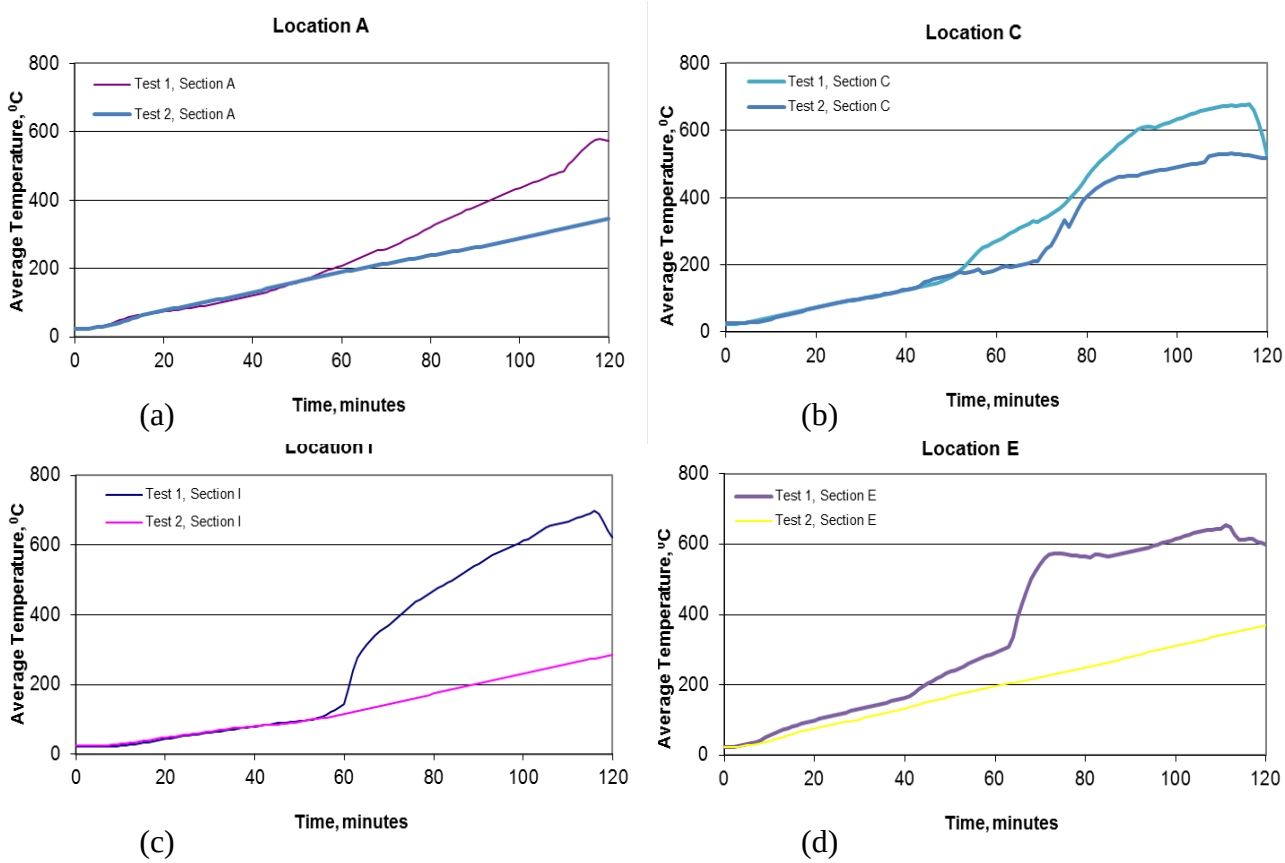

Figure 9 (a) through (d): Comparison of two average temperatures in the top chord in Test 1 and 2.

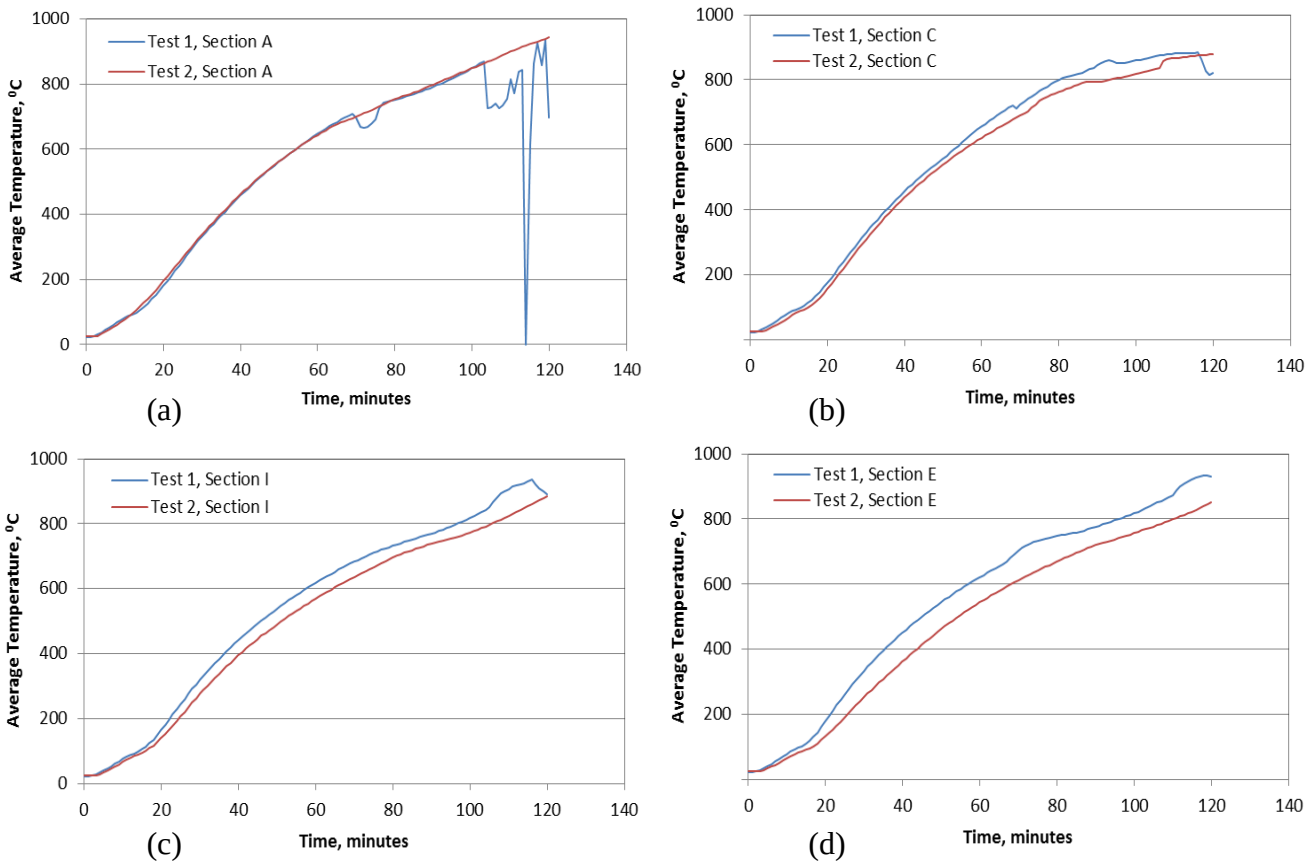

Figures 10 (a) through (d): Comparison of two average temperatures in the mid-web regions for Test 1 and 2.

3.5 Variability in Experimentally Recorded Temperatures

There is significant variation in recorded temperatures along the top chord, (a) in the same position (A 1 and A 5 in Test 1) (Figure 11(a)), (b) in the same location at two main trusses (A 1 and B 1) (Figure 11(b)), and (c) at different locations along a truss length (A1 and E1) (Figure 11(c)). Such wide difference in recorded temperatures indicates the need to determine the variability in the time-dependent, non-uniform temperature distribution in steel members. It is important to determine the factors that could possibly contribute to this variability. Some of these are: a) non-uniform heating as a result of varying gas temperatures based on locations, b) time-dependent change in “view factors” due to concrete spalling or SFRM buildup, c) change in net convective heat transfer due to changes in local gas temperatures near the vicinity of the thermocouples. The second phase of this research will attempt to compute uncertainties in temperatures and compare with those obtained in measurements.

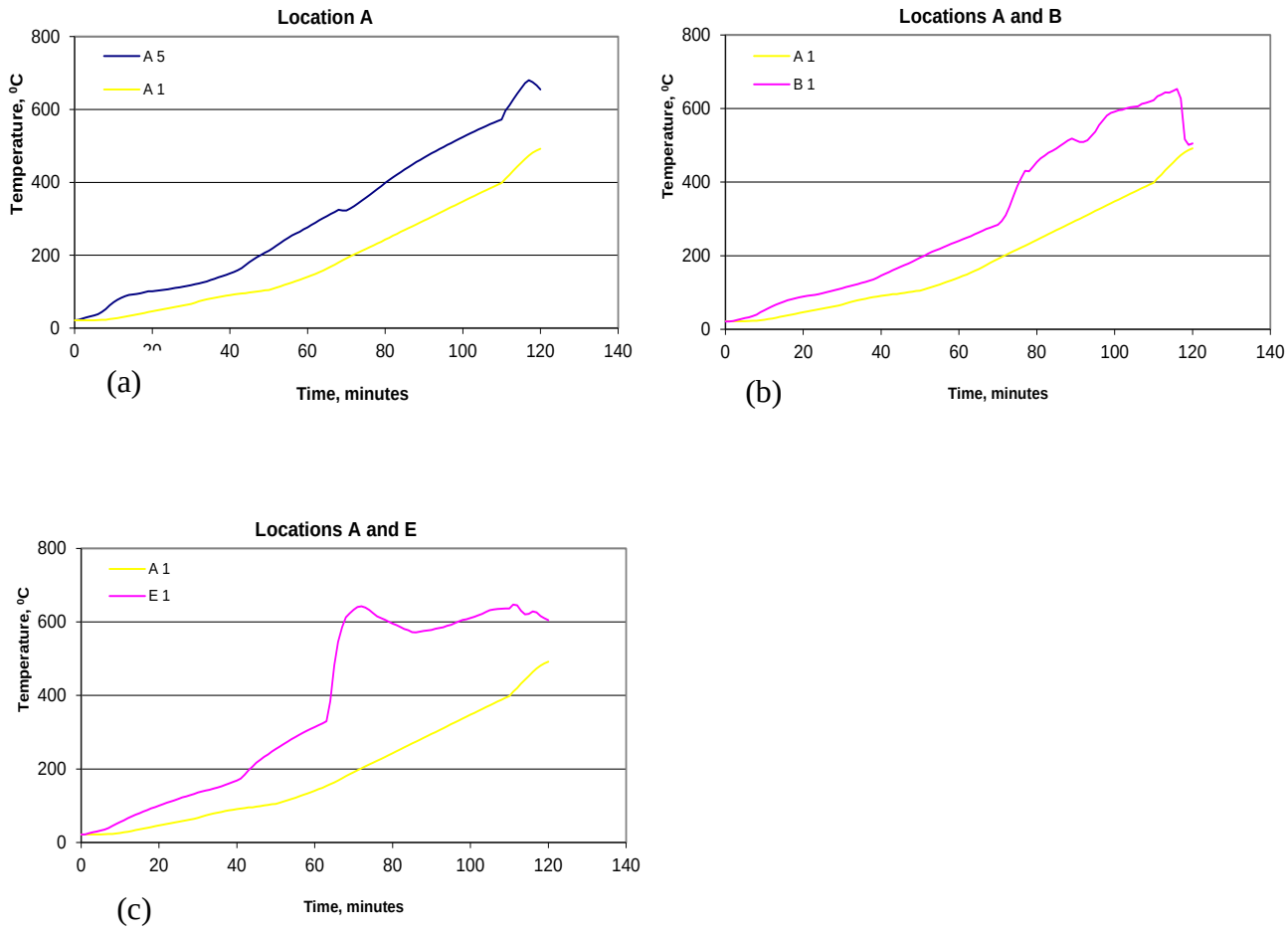

Figure 11: Comparison of experimentally recorded temperatures in Test 1 for top chord locations.

Table 1 lists the means and standard deviations of the average measured temperatures at lower chord, mid-web, and upper chord locations for the two main trusses for two different times (60 minutes and 120 minutes into the test). Recall that the data were recorded at 10 locations along the two main trusses (A, G, C, I, and E in the north main truss and B, H, D, J, and F in the south main truss; see Figure 2). At each location, two thermocouple readings were available at the top chord and mid-web, while four readings were available at the bottom chord. Average of these temperature readings at the top chord, mid-web, and the bottom chord were calculated at each of the 10 locations along the two main trusses. Then, the overall mean temperatures and the standard deviations at the top chord, mid-web, and the bottom chord were computed considering these 10 average temperatures for both tests. In computing these data, anomalous thermocouple readings were excluded.

These data are plotted in Figure 12. The mean temperature data show that the web members heated up the fastest for both tests. This is expected since a) heating of the web can be considered to be uniform and the influence of the floor slab is presumed to be minimal b) the exposed surface area/volume ratio of web members are greater than that of the chord members. The pattern of heating for the two tests shows similar trends. Also, the mean temperatures in the lower chord, mid-web, and upper chord of the truss in both the tests are reasonably close. Clearly, Test 1 showed wide variability in mean temperatures (see standard deviations for Test 1 in Table 1). This is likely due to the concrete spalling as discussed earlier. This event changed the subsequent thermal profile in the truss, contributing to variability in recorded temperatures. The upper chord mean temperature at 120 minutes was about 33 $^{\circ}$C higher in Test 1 than in Test 2.

Table 1. Means and standard deviations of average temperatures at three locations on the main truss in tests 1 and 2 at 60 minutes and 120 minutes into the fire.

Location on	60 minutes				120 minutes			
	Test 1		Test 2		Test 1		Test 2	
main truss	μ, ^{0}C	σ, ^{0}C	μ, ^{0}C	σ, ^{0}C	μ, ^{0}C	σ, ^{0}C	μ, ^{0}C	σ, ^{0}C
Lower Chord	445.7	81.8	446.4	54.3	773.3	69.8	772.0	37.9
Mid Web	600.4	35.0	576.5	36.6	860.3	70.3	872.2	42.9
Upper Chord	161.3	35.4	162.9	29.0	358.1	108.6	325.4	39.5

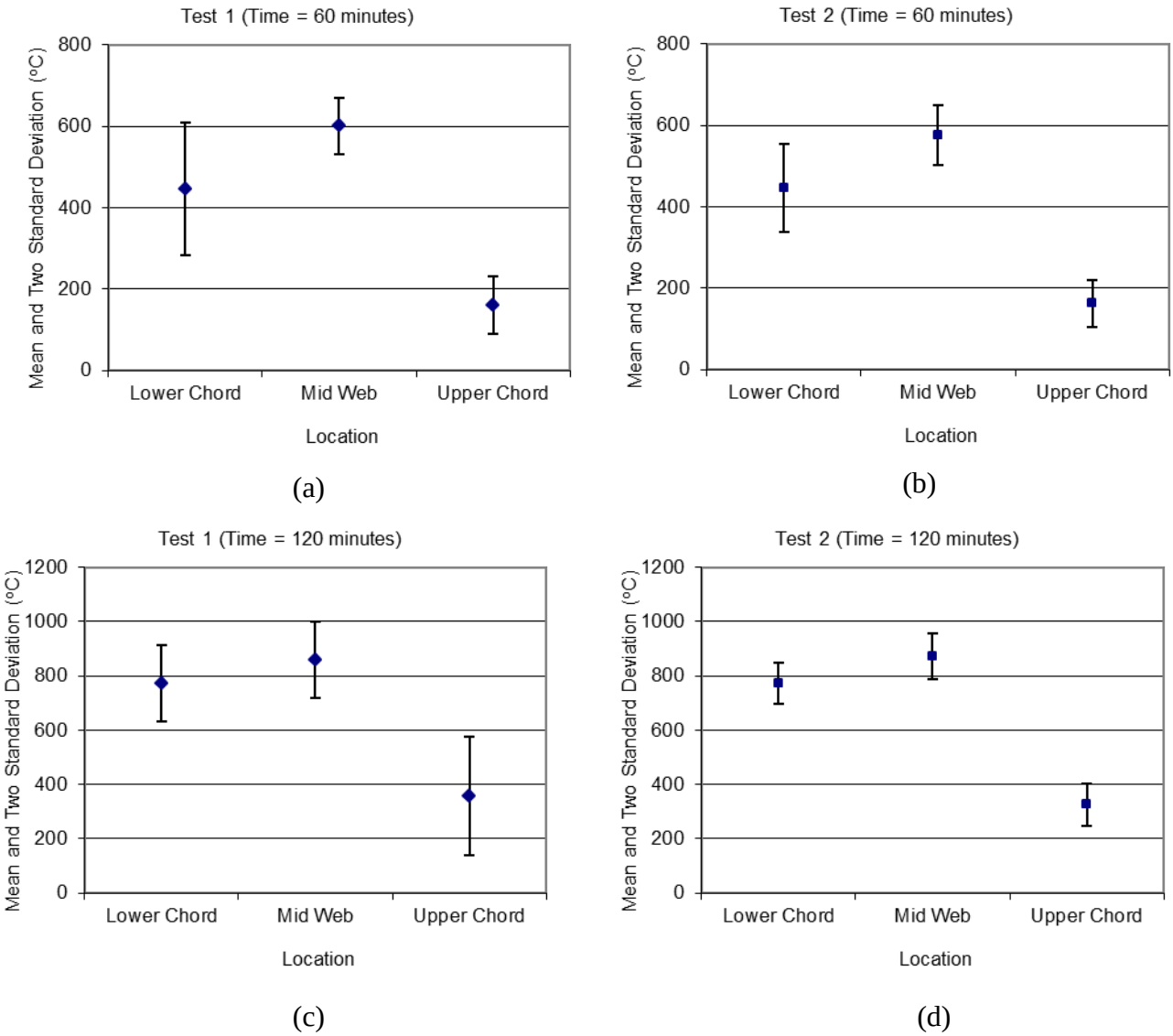

Figure 12: Mean temperatures and two standard deviations at 3 locations on main trusses in tests 1 and 2 at 60 minutes (a, b) and 120 minutes (c, d) into the tests.

The measured temperatures at 4 locations show that the difference between the average temperatures at the top chord and mid-web positions was: 218 ˚C at 30 minutes and 502 ˚C at 2 hours in Test 1 respectively and 200 ˚C at 30 minutes and 546 ˚C at 2 hours in Test 2 respectively. The difference between the average temperatures at the top chord and bottom chord positions were: 95 ˚C at 30 minutes and 415 ˚C at 2 hours in Test 1 respectively and 105 ˚C at 30 minutes and 446 ˚C at 2 hours in Test 2 respectively.

Additionally, the measured temperatures at 4 locations also show that the maximum differences between the average temperatures along the member length were:

- 34 °C and 76 °C at the mid-web at 30 minutes and 90 minutes respectively in Test 1 and 85 °C and 79 °C at the mid-web at 30 minutes and 90 minutes respectively in Test 2.
- 74 °C and 124 °C at the bottom chord at 30 minutes and 90 minutes respectively in Test 1 and 38 °C and 167 °C at the bottom chord at 30 minutes and 90 minutes respectively in Test 2.
- 46 °C and 128 °C at the top chord at 30 minutes and 90 minutes respectively in Test 1 and 38 °C and 77 °C at the top chord at 30 minutes and 90 minutes respectively in Test 2.

These data indicate that the time-dependent variation of temperatures along the length of a member must be considered in conducting structural analysis during fire tests. One conclusion that can be drawn from the above discussion is that concrete spalling contributes significantly to the overall uncertainty in steel member temperatures. Variabilities in member thermophysical properties, fire/member heat exchange parameters, and gas temperatures must be considered to determine the overall uncertainties in member temperatures.

4 Heat Transfer Modeling

A finite element model of the composite floor system described in section 2.1 was developed using the ANSYS finite element software. The dimensions of the model were taken from Ref. [2]. The purpose of the heat transfer model is to simulate the transient heat diffusion in the fire-exposed composite floor system. The heat transfer model was used to compare model predictions of temperatures at a few locations in the floor system with experimental measurements. Thermal data predicted by this validated heat transfer model will be later used in a structural analysis model for predicting the time-dependent behavior of the floor system due to both thermal and gravity loads.

In this section, the following topics are covered:

1) Details of the methodology used to develop the heat transfer model
2) Description of input data used for thermophysical properties of materials in the floor system and the boundary and initial conditions
3) A brief description of the approach used to interpolate temperature values (which are compared with experimental measurements)

4.1 Methodology

A finite element model of the composite floor system shown in Figure 2 was constructed by including the following:

a. One steel main truss (without end supports) including the top chord, web diagonals, and the bottom chord.
b. Concrete slab (above the main truss) spanning the entire truss length and half the furnace width of 2.15 m (see Figure B1 in Appendix B).

Note that only one main truss shown in Figure 2 was modeled in this study. Bridging trusses were not included. The spray applied fire resistive material (SFRM) was considered to be uniformly applied over the steel truss (no fireproofing was applied on the top surface of the top chord). Additionally, the exposed surface of the slab was assumed to have an overspray of SFRM of about 19 mm. Note that the profiled steel metal deck was not specifically modeled since the metal deck is only 0.9 mm thick, while the slab is about 130 mm thick. Moreover, Lamont's [6] results did not show a significant difference in the temperature prediction in the slab when a metal deck was specifically modeled in comparison with the case when the metal deck was not included.

The finite element model of the composite floor assembly was developed using 3-D solid thermal elements (SOLID 70 element in ANSYS), which have eight nodes with a single degree of freedom (temperature) at each node. The truss upper chords and lower chords were connected with the web members using conduction link elements (Link 33 element in ANSYS). These are uniaxial elements that can be used to model the transient heat transfer between the end nodes. Use of link elements allows the diagonals to be meshed independently of the upper and lower chords and resulted in the minimum possible volumes in the model. Figures B1 and B2 (Appendix B) show the FE (finite element) model in detail. Note that adequate numbers of elements had to be used through the depth of each material to ensure that at least two free nodes existed at each section and that steep thermal gradients, if any, are handled correctly in the model.

During fire exposure, heat exchange occurs by both convection and radiation. At higher temperatures, radiation plays a more dominant role in thermal exchange. The convective heat exchange is addressed by the Newtonian heating/cooling mechanism. The radiative heat exchange is defined by the Stefan-Boltzmann law, which includes a parameter called "view factor". The view factor is defined by the proportion of the radiation that leaves a surface (e.g., surface A) that strikes another surface (e.g., surface B). It can assume values from 0 to 1.

In order to simulate the furnace heating in the UL tests, the exposed surfaces of the composite floor system were subjected to convective and radiative heat exchanges. In order to accomplish this, surface effect elements were generated in ANSYS and overlaid on the exposed surfaces of the solid elements. This is because only one type of thermal surface load can be applied to a given entity in ANSYS. For example, one cannot apply both a flux and a convection boundary condition directly to the faces of an element. Surface effect elements allow the use of multiple surface loads to a given element face. Two types of surface effect elements were created: one for the convective heat exchange and the other for the radiative heat exchange. All of these surface effect elements were created with a particular reference node. For the convective surface elements, the fluid

bulk temperature was designated as that of the reference node and appropriate convective heat transfer coefficients were used (see the next section). For the radiative heat exchange, surface effect elements were created with a reference node. An imposed temperature constraint (e.g., furnace heating following the ASTM E119 curve) was specified on this node. A resultant emissivity value was specified while creating these surface effect elements. The resultant emissivity includes proper emissivity values of the receiving and emitting surfaces. View factor effects in the radiation heat transfer were not considered, since the furnace was not explicitly modeled in this study and therefore, view factor values were set to 1 for all elements.

4.2 Thermophysical Properties, Boundary and Initial Conditions

Thermophysical properties for materials used in the model (e.g., steel, concrete, and SFRM) are taken from Ref. [7] and are listed in both tabular and graphical forms in Appendix A. Note that temperature-dependent values of materials properties were used. The three thermophysical properties that are needed for thermal analysis are: density, specific heat, and thermal conductivity.

Proper boundary conditions are needed to model the heat transfer to/from the floor system both at the exposed and unexposed surfaces (e.g., at the bottom and top surfaces of the slab). For the convective surface effects elements at the exposed surface, a convective heat transfer coefficient is specified. A value of 25 $W/m^2/K$ has often been used [8]. Lamont et al. [6] used a base value of 23 $W/m^2/K$, with minimum and maximum values of 5 $W/m^2/K$ and 30 $W/m^2/K$ in their sensitivity analysis. Lamont et al. suggested using a lower value of this heat transfer coefficient when the profiled metal deck is not explicitly modeled. This is because the profiled metal deck is known to separate from the rest of the concrete slab during progression of a fire event, thereby creating a gap that reduces the convective heat transport at the exposed surface of the slab. In this analysis, a value of 15 $W/m^2/K$ was used for the convective heat transfer coefficient since the profiled metal deck was not modeled this study.

The effective emissivities for radiative heat exchange at the exposed surface depend on many factors such as flame emissivity, compartment walls, etc. For the surface emissivity of the steel member, a value of 0.7 is used. At the exposed surface of the slab, a value of 0.6 is used for effective emissivity as recommended by Lamont [6]. This value is slightly different from that of steel and was used as the metal deck was not explicitly modeled in this study. This is because of the air gap that forms at the interface between metal deck and concrete slab. Lamont found very good agreement between modeled and measured concrete slab temperatures when this value of emissivity was used.

Note that adiabatic boundary conditions were maintained at each end of the model in the longitudinal direction of the truss. Average time-temperature values for different segments on the unexposed surface of the concrete slab as determined from recorded thermocouple data during the two fire tests were used as Dirichlet boundary conditions (time varying) for nodes on the unexposed surface of the concrete slab. Note that this

boundary condition is the only difference between Test 1 and Test 2 from the thermal modeling perspective. All nodes in the model were assigned an initial temperature of 25 °C. The input temperatures to the model are the ASTM E119 time-temperature curve assigned to the reference node as described in the previous section. This essentially assigns the furnace heating to this reference node. All exposed surfaces exchange convective and radiative heating with this node.

4.3 Interpolation of Temperatures

The numerical model predictions can be compared with measured time-temperature data at locations A, C, E, and I along the main truss (see Figure 2). These comparisons are performed at the upper chord, mid-web, and the lower chord for these four locations. However, often there is not a node at the exact location where a thermocouple was positioned. In order to obtain a simulated temperature at the measurement point, interpolation of temperatures was done as described in the following paragraphs.

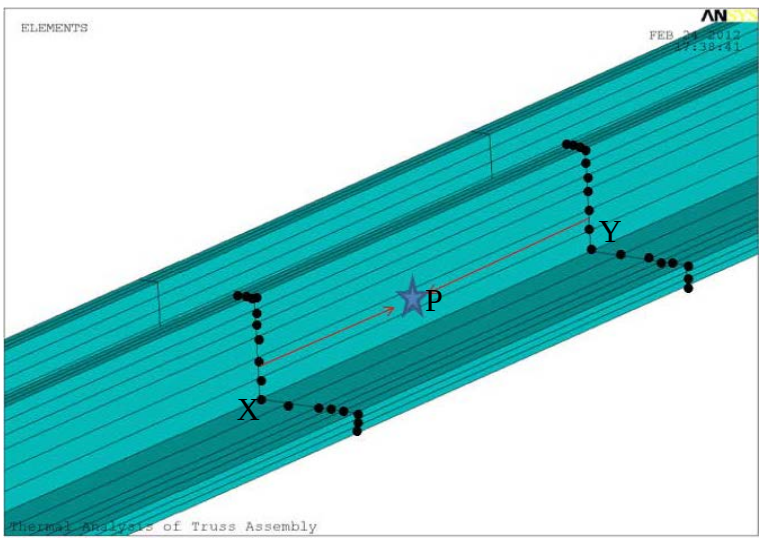

Figure 13. Schematic illustration of the averaging approach used to interpolate temperatures.

The model predictions of temperature at a given location along the truss (e.g., A, C, E, or I in Fig. 2) are obtained as shown schematically in Figure 13. For example, temperature at the position of interest (e.g., P at the bottom chord in Figure 13) is obtained by taking a weighted average of temperatures of all the FEM nodes available nearest to the point P on either side. In other words, first average temperatures at X and Y are obtained by finding the mean temperatures of all the nodes at X and Y (e.g., through the entire sections at X and Y). Then the temperature at the point of interest (P) is estimated by finding a weighted average of computed mean temperatures at X and Y using the proper distance of P from both locations X and Y. A script was written in ANSYS parametric design language (APDL) to output these temperatures as functions of time for the desired locations along the truss for upper chord, mid-web, and lower chord positions. These

temperatures were then compared with measured temperatures available for these locations.

5 Evaluation of the Heat Transfer Model

In this section, average computed time-temperature data at four selected locations along (A, C, E, and I) the North Main Truss are compared against the experimentally obtained results in both the tests. As mentioned earlier, these measurements were taken at bottom chord, mid-web, and upper chord positions at five locations along each main truss. Whenever experimental data showed anomalous temperatures, readings from the South Main Truss for the identical location have been included in plots for comparison. Additionally, erroneous thermocouple data have not been included. Note that erroneous thermocouples are listed in the log of experimental data as reported in ref [2].

5.1 Test 1

Figures 14, 15, and 16 show comparisons between ANSYS predicted mean temperatures and measured temperatures at these four locations along the north main truss for positions at bottom chords, mid-webs, and top chords (see Figure 2 for labeling of positions).

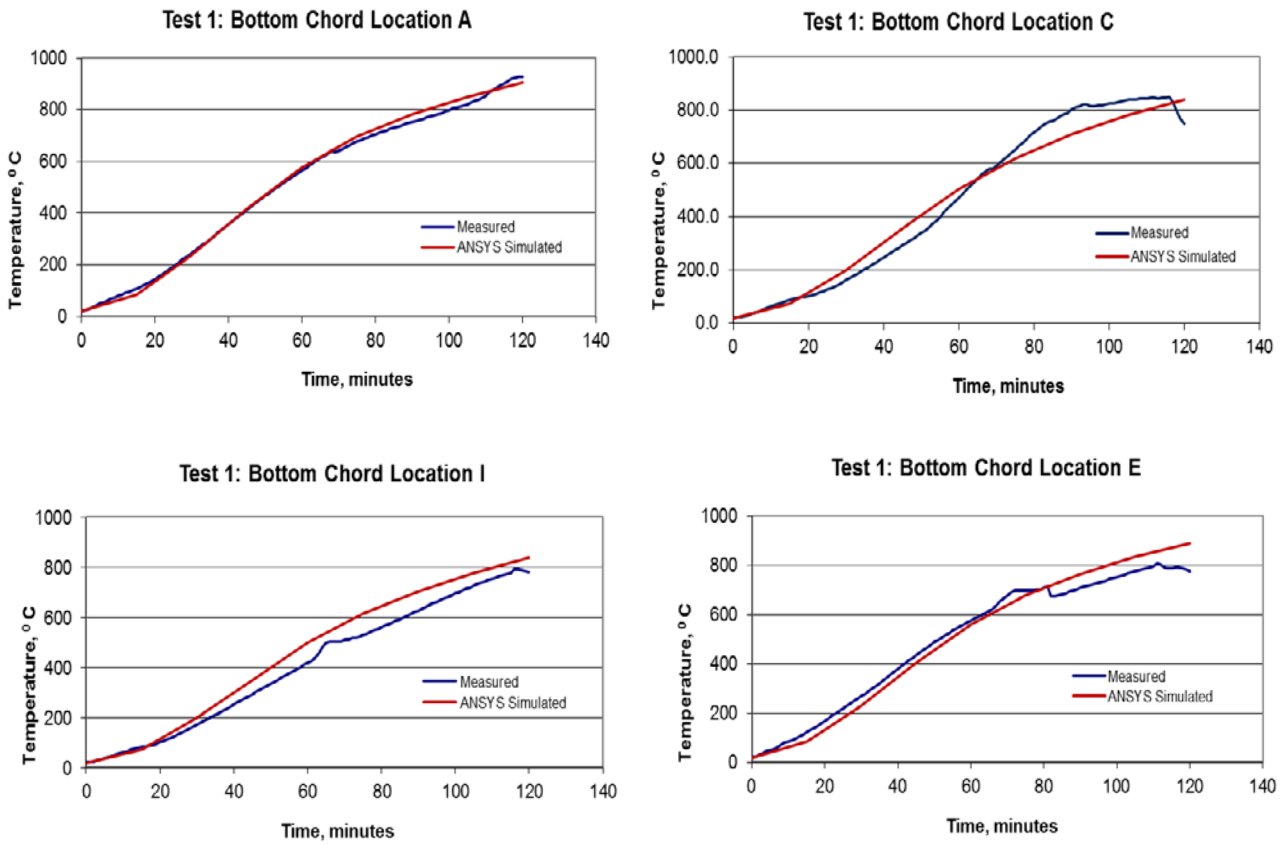

Figure 14: Time-temperature plots of the thermocouple data recorded for the bottom chord at four locations on the north main truss in UL Test 1. Also shown are the average computed temperatures obtained from ANSYS.

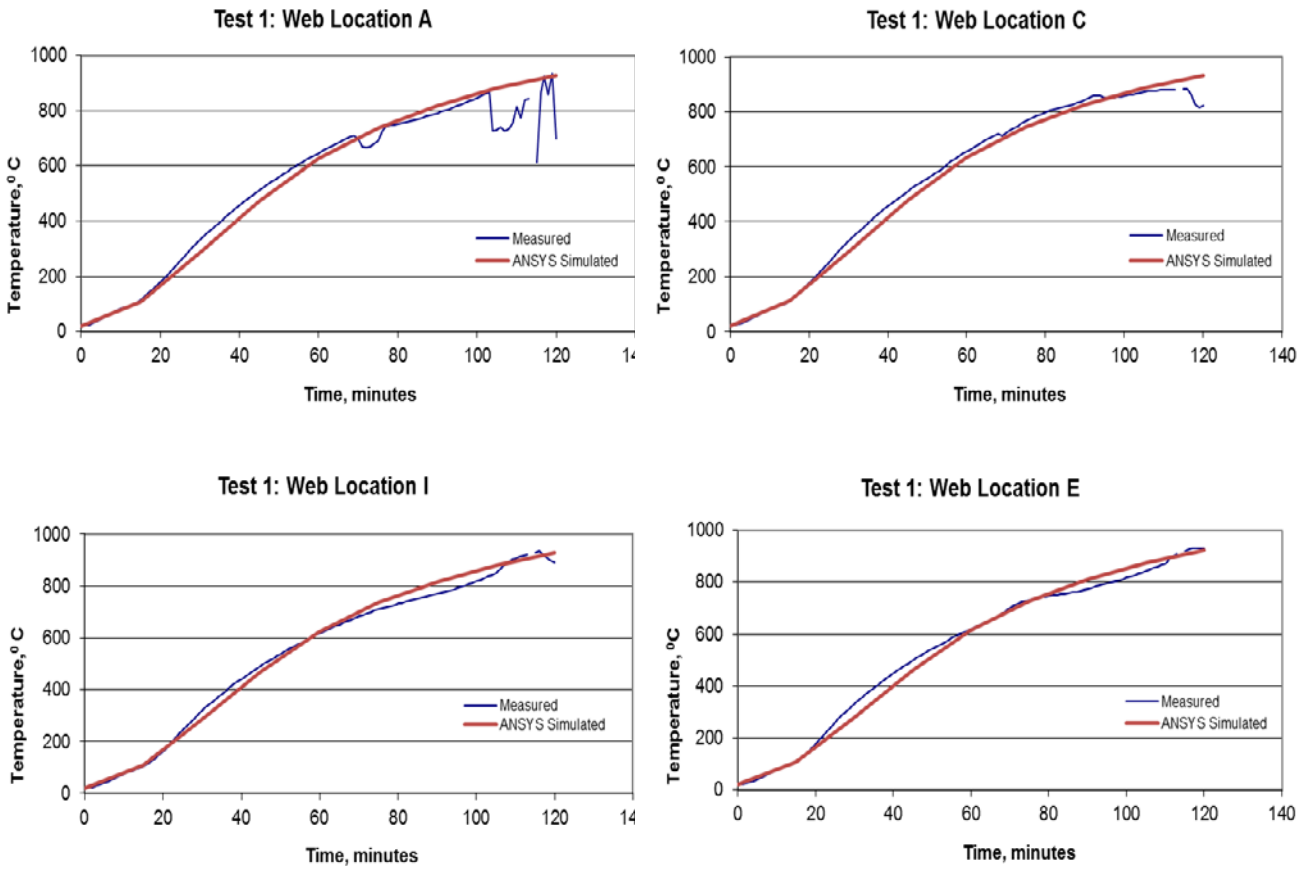

Figure 15: Time-temperature plots of the thermocouple data recorded for the mid-web position at four locations on the north main truss in UL Test 1. Also shown are the average computed temperatures obtained from ANSYS.

Table 2 shows a listing of measured and ANSYS computed temperatures for four different times during the test at the lower chord, mid-web, and upper chord for the four locations along the truss. Additionally, percentage differences of computed temperatures (in absolute scale e.g., K) from experimental values are also listed. It is evident that the agreement is good for both bottom chord and mid-web locations except for the location I at the bottom chord, where the difference between the measured and computed temperatures was as high as 12%. Such disagreement is also present in Test 2 as will be discussed later.

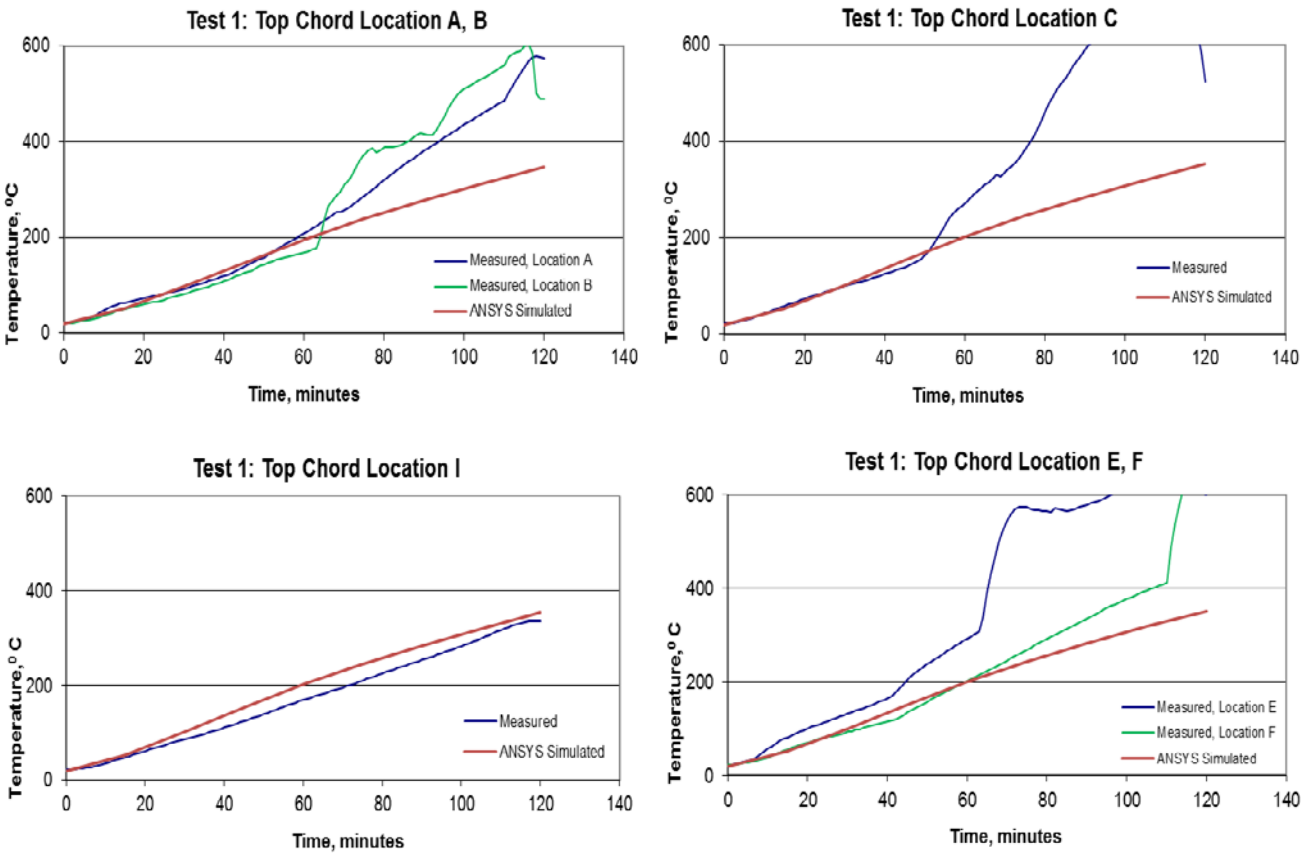

Figure 16: Time-temperature plots of the thermocouple data recorded for the top chord position at four locations on the north main truss in UL Test 1. Also shown are the average computed temperatures obtained from ANSYS.

A loud report was heard at 45 minutes (see Appendix C) when concrete spalling occurred, resulting in dislodgement of fireproofing from the top chord (see Ref [2]). This resulted in an abrupt rise in steel temperatures as shown by the experimental plots for the top chord (Figure 16). These plots show that the thermal model has been set up correctly since the initial rate of heating matches closely with the rate shown in the measured curves. Moreover, Table 2 shows that the agreement is within 10% for most mid-web and bottom chord locations. Another observation can be made from Table 2: the discrepancies between measured and computed temperatures for mid-web and lower chord positions are somewhat large during the initial periods of the test. This discrepancy may be attributed to the fact that the model includes only one truss and transient effects due to non-uniform heating and heat exchanges between members such as bridging trusses, and the south main truss were not included here. This discrepancy diminishes at later times into the test as gas temperatures became more uniform in the furnace.

Table 2: A comparison of experimental and predicted temperatures at four times for Test 1.

Test1												
Mid Web	Temperatures in C (% diff in absolute scale (K))											
Time, min	**Exp (A)**	**ANSYS (A)**	**% diff**	**Exp (C)**	**ANSYS (C)**	**% diff**	**Exp (I)**	**ANSYS (I)**	**% diff**	**Exp (E)**	**ANSYS (E)**	**% diff**
30	331	285	-7.7	299	289	-1.7	320	285	-5.8	332	280	-8.6
60	647	626	-2.2	656	633	-2.4	618	625	0.7	621	617	-0.4
90	792	820	3.5	846	826	-1.8	770	817	4.5	775	811	3.4
120	-	929	-	-	934	-	899	927	2.4	933	923	-0.9
Bot Chord												
Time, min	**Exp (A)**	**ANSYS (A)**	**% diff**	**Exp (C)**	**ANSYS (C)**	**% diff**	**Exp (I)**	**ANSYS (I)**	**% diff**	**Exp (E)**	**ANSYS (E)**	**% diff**
30	245	237	-1.7	180	200	4.5	172	198	5.8	195	229	7.4
60	565	578	1.5	477	502	3.4	417	498	11.7	461	561	13.6
90	752	782	2.9	747	709	-3.7	628	704	8.5	735	765	3.0
120	929	903	-2.1	-	841	-	781	838	5.3	768	889	11.6
Top Chord												
Time, min	**Exp (A)**	**ANSYS (A)**	**% diff**	**Exp (C)**	**ANSYS (C)**	**% diff**	**Exp (I)**	**ANSYS (I)**	**% diff**	**Exp (E)**	**ANSYS (E)**	**% diff**
30	92	97	1.3	100	101	0.5	86	102	4.3	132	100	-7.9
60	209	196	-2.7	-	203	-	169	203	7.5	-	151	-
90	382	278	-	-	284	-	254	284	5.8	-	282	-
120	574	348	-	-	353	-	336	353	2.8	-	351	-

5.2 Test 2

Table 5-5 of Ref. [2] indicates that it took 76 minutes of heating for average steel temperatures in Test 2 to reach 593.3 ˚C (time to reach End-point Criteria in ASTM E 119 test), while this duration was 66 minutes for Test 1. These data indicate that the heating rate in steel members was slower in Test 2 that it was in Test 1. This is also evident in Figures 8, 9, and 10, where average temperatures recorded in the two tests along a main truss are compared. Factors such as heat loss could play a role in somewhat reduced steel member heating rates seen in Test 2. Moisture level in concrete can also play a role as a concrete slab with higher moisture content is expected to be a more effective heat sink.

Figures 17 through 19 compare measured and predicted steel temperatures at lower chord, mid-web, and upper chord positions along the length of the truss. It can be noticed that measured bottom chord temperatures for most locations are slightly lower than predicted temperatures. The agreement at the bottom chord is within 10%. The agreement at mid-web position is generally within 5%. For upper chord, the agreement is within 4% except at location I. This discrepancy can also be seen in Table 3, where measured and predicted temperatures are listed at four different times during the fire test.

As seen in Test 1, the measured temperatures at location I in Test 2 are substantially lower than those predicted by the model. The reason behind this is not quite clear. One possible explanation is that since the bridging truss intersects the main truss at location I (see Figure 2), it could act as heat sink. It may be noted that although the bridging truss was heated during the tests, it could still act as a heat sink because of its thermal mass. Since the bridging truss was not included in the model, this discrepancy could not be addressed. In the future, the computational model will include the entire floor system (e.g., both main trusses and bridging trusses).

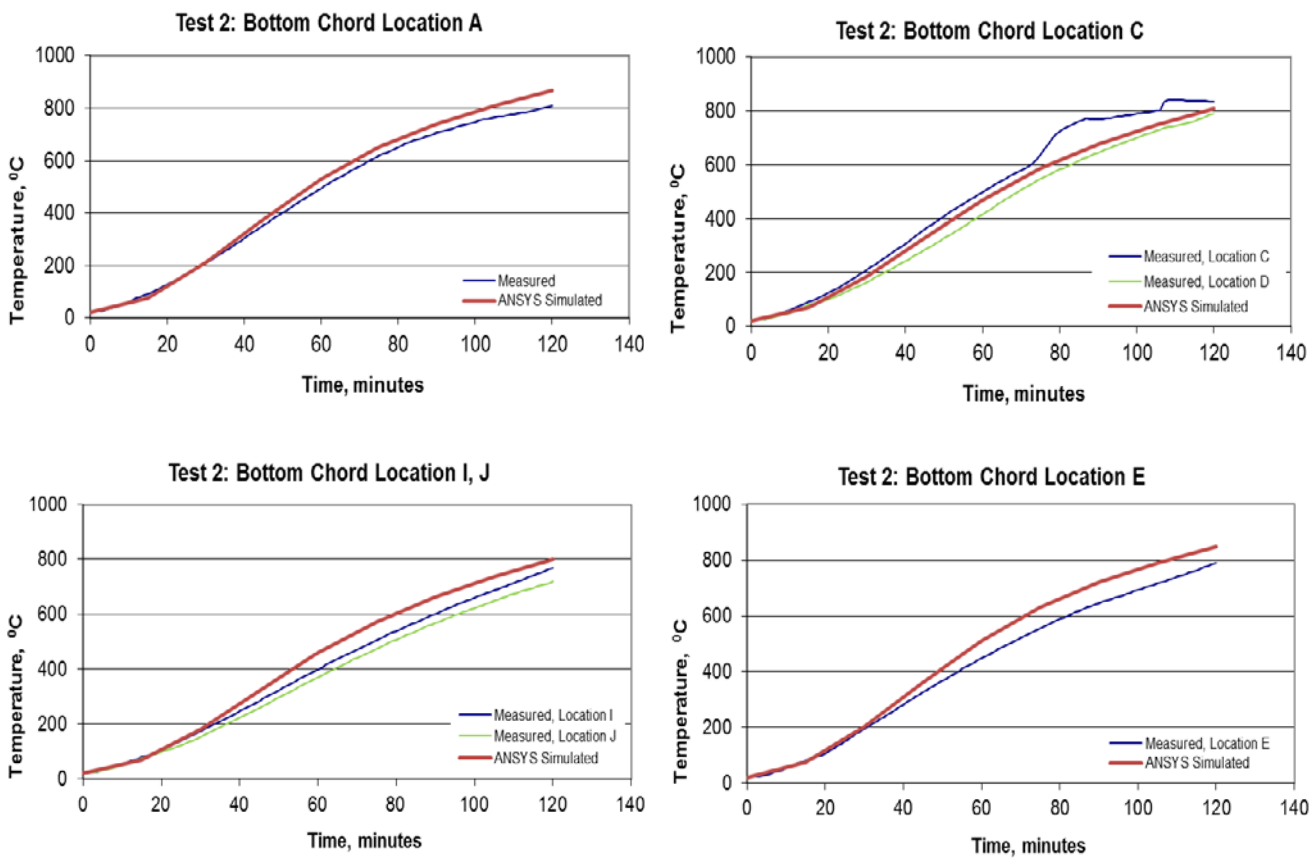

Figure 17: Time-temperature plots of the thermocouple data recorded for the bottom chord at four locations on the north main truss in UL Test 2. Also shown are the average computed temperatures obtained from ANSYS.

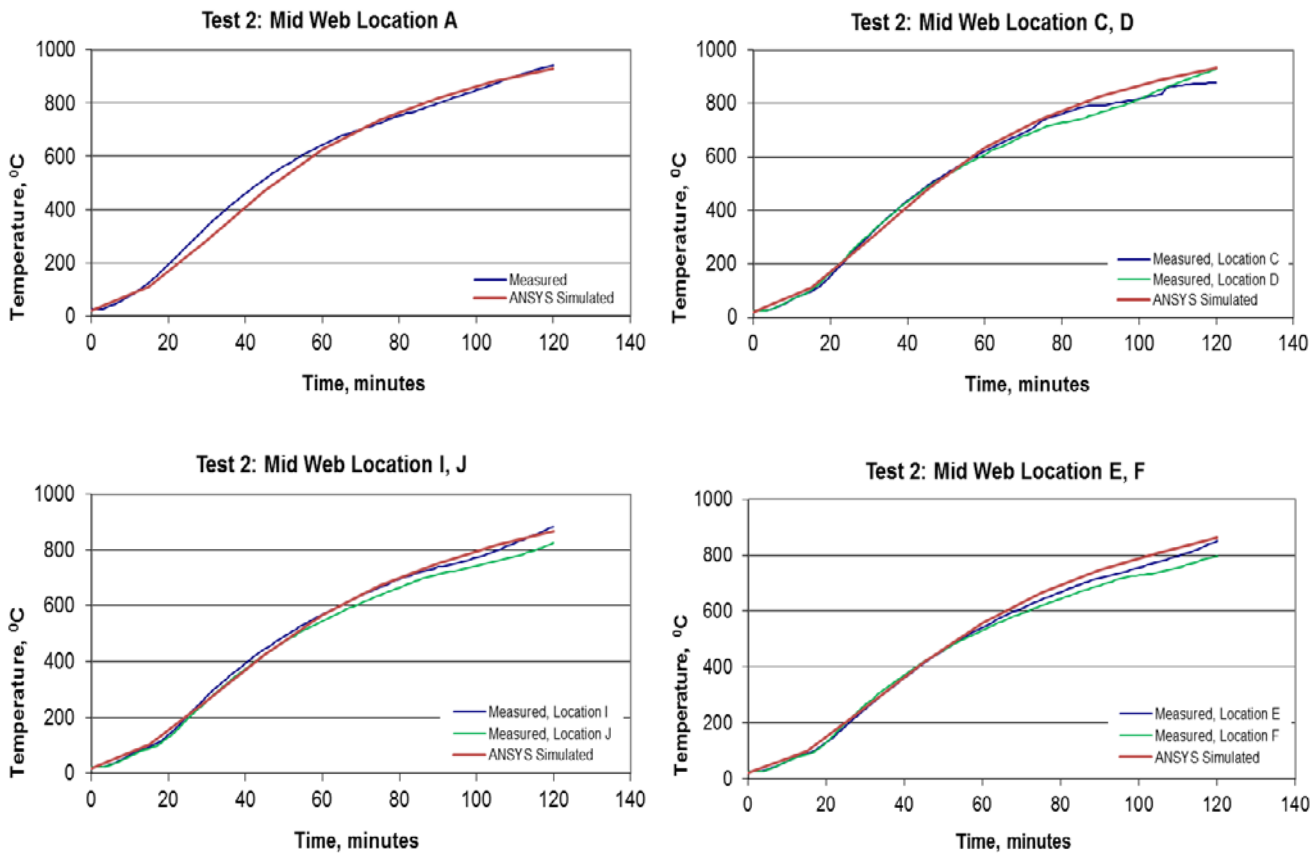

Figure 18: Time-temperature plots of the thermocouple data recorded for the mid-web at four locations on the north main truss in UL Test 2. Also shown are the average computed temperatures obtained from ANSYS.

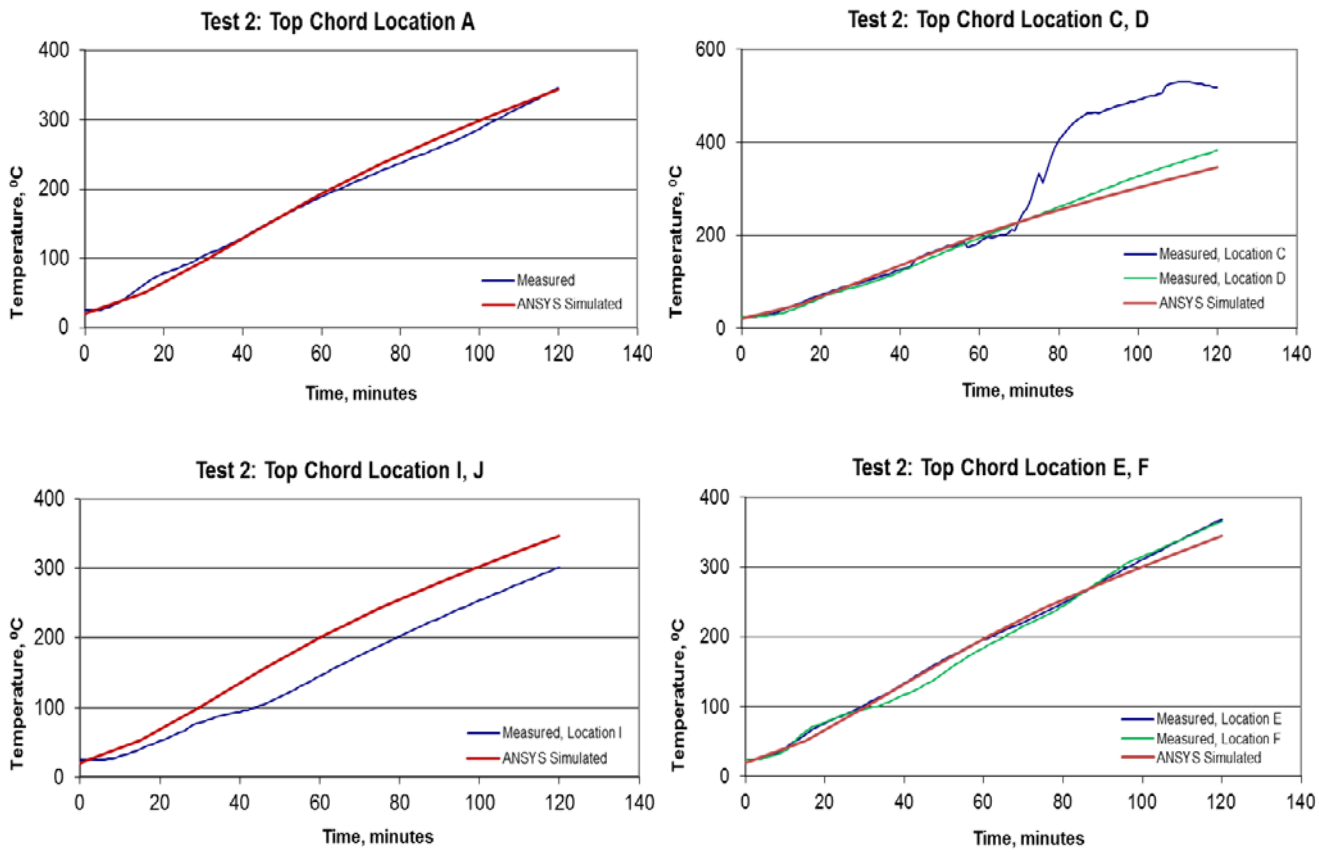

Figure 19: Time-temperature plots of the thermocouple data recorded for the top chord at four locations on the north main truss in UL Test 2. Also shown are the average computed temperatures obtained from ANSYS.

Table 3: A comparison of experimental and predicted temperatures at four time levels for Test 2.

Test2

Mid Web Temperatures in ^{0}C ((% diff in absolute scale (K))

Time, min	Exp (A)	ANSYS (A)	% diff	Exp (C)	ANSYS (C)	% diff	Exp (I)	ANSYS (I)	% diff	Exp (E)	ANSYS (E)	% diff
30	337	284	-8.6	308	289	-3.2	276	259	-3.1	252	255	0.6
60	643	626	-1.9	621	633	1.4	569	566	-0.4	543	559	1.9
90	798	819	2.0	793	825	3.1	738	753	1.5	720	746	2.7
120	943	929	-1.1	879	934	4.7	884	867	-1.4	852	862	0.9

Bot Chord

Time, min	Exp (A)	ANSYS (A)	% diff	Exp (C)	ANSYS (C)	% diff	Exp (I)	ANSYS (I)	% diff	Exp (E)	ANSYS (E)	% diff
30	210	211	0.3	211	185	-5.3	173	181	1.7	195	204	1.9
60	495	530	4.5	498	469	-3.7	399	459	9.0	447	512	9.0
90	705	739	3.5	769	676	-8.9	602	664	7.1	646	720	8.0
120	808	868	5.6	835	810	-2.3	768	798	2.9	791	850	5.6

Top Chord

Time, min	Exp (A)	ANSYS (A)	% diff	Exp (C)	ANSYS (C)	% diff	Exp (I)	ANSYS (I)	% diff	Exp (E)	ANSYS (E)	% diff
30	104	97	-2.0	98	100	0.6	66	101	10.4	103	99	-1.0
60	189	194	1.0	186	200	3.2	116	200	21.8	196	198	0.4
90	261	275	2.7	-	280	-	203	280	16.2	280	277	-0.4
120	346	345	-0.2	-	346	-	285	346	11.0	369	344	-3.9

5.3 Effect of SFRM Dislodgement

As shown in Figure 9(a) through 9(d), the top chord temperatures for the two tests show similar heating trends on average. However, the reduction in the thickness of SFRM as a result of dislodgement possibly resulted in the sudden increase in the recorded temperatures for a few locations for Test 1. The aim in this section is to demonstrate an approach for estimating the effect of SFRM dislodgement at specific locations.

The analysis of Test 1 showed significant effects of concrete spalling on temperatures at the top chord (Figure 9). ANSYS simulation was interrupted according to the timeline corresponding to the loud reports indicated in the log of observations [Appendix A and B] and 2 ft. (0.61 m) to 3 ft. (0.91 m) of SFRM in length were removed from the model at these locations. ANSYS simulation was then restarted and continued until the occurrence of the next loud report. A trial and error approach was followed to determine the range of possible amounts of SFRM dislodgement presumed to occur at each location. A schematic of SFRM dislodgement from the model is shown in Figure 20.

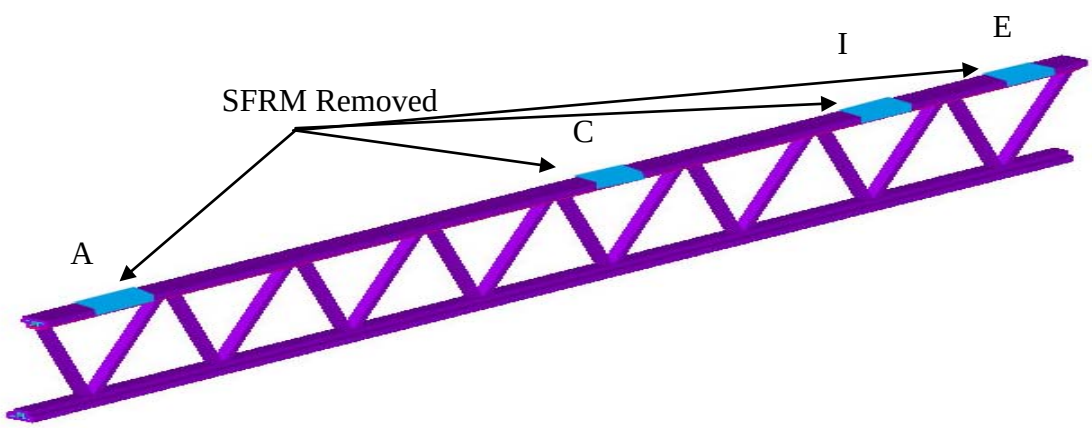

Figure 20: A schematic of the SFRM removal at locations A, C, I, and E in Test 1.

For Test 1, at 3800 s, 0.5 in. (12.7 mm) of SFRM was removed at location A and 0.75 in. (19 mm) of SFRM was removed at locations I and E. Simulation was then restarted and continued until 4500 s, when 0.75 in. (19 mm). of SFRM was removed at location C and then simulation was restarted. Figure 21 shows a comparison of computed and experimental data at the four locations along the top chord in Test 1. For locations C and E, computed results are also shown for the hypothetical case of SFRM remaining intact. As expected, the temperature plots (for this case of SFRM remaining intact) continue along the “ANSYS simulated, SFRM removed” curves before abrupt heating took place during the onset of dislodgement of SFRM (see dashed plots for ANSYS simulation for locations C and E in Figure 21).

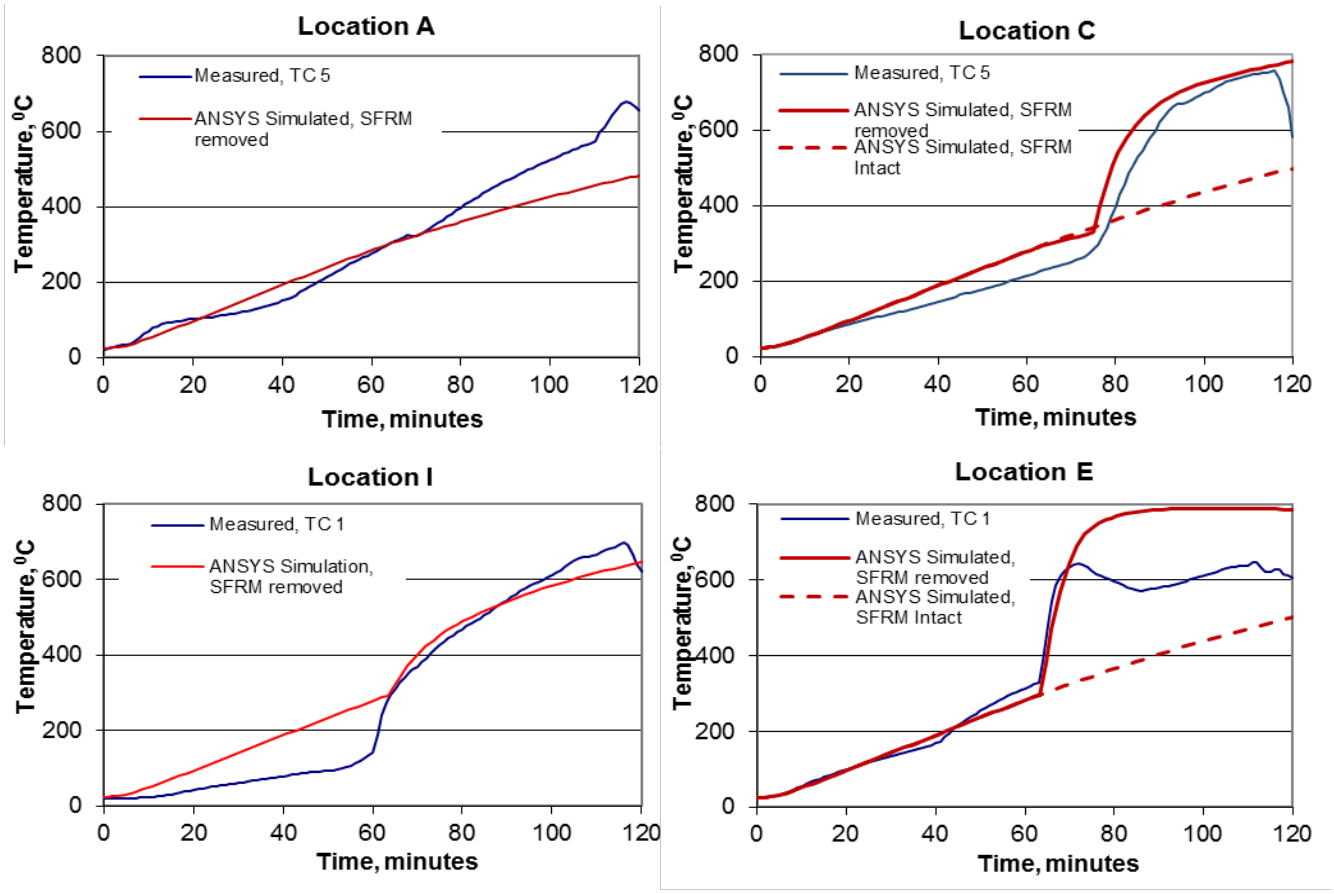

Figure 21: Comparison of numerical results and experimental data for upper chord temperatures in Test 1 with SFRM removal.

It can be seen that the average computed temperatures match reasonably well with the thermocouple data at location A. At location C, the computed rate of heating was higher than that of the experimental plot. This is true until about 75 minutes when there is an abrupt temperature increase possibly due to dislodgement of SFRM from steel. There is a reasonable match between the computed and experimental data at location E except toward the end, when the experimental data show a dip in temperature followed by a gradual increase toward the end. This analysis shows that it is possible to estimate the extent of SFRM dislodgement from steel members during a fire exposure by conducting a controlled and iterative modeling exercise such as the one shown here.

6 Summary

An analysis of the measured temperatures of the main trusses in the two full-scale fire resistance tests showed that the steel web members heated faster than the bottom and top chord members and at the end of the test, the steel web members recorded the highest temperatures. On the whole, the restrained test (Test 1) showed higher variability in recorded steel temperatures than that in the unrestrained test (Test 2). This is because there was less cracking and spalling of concrete in the unrestrained test. Additionally, top chord temperatures in the restrained test showed wide variability especially toward the end of the fire tests. This conclusion can be drawn based on large values of standard deviations obtained.

An ANSYS heat transfer model was developed with appropriate thermophysical properties and model parameters (e.g., boundary conditions, initial conditions etc.) to predict the thermal behavior of the structural members. The heat transfer model was evaluated by comparing the time-dependent evolution of measured mean temperatures at lower chord, mid-web, and upper chord positions along four specific locations of the main trusses with average computed temperatures. For the bottom chord and mid-web locations, the agreement between measured and ANSYS temperatures was within 15% for both tests. For the top chord, the agreement was within 10% until about 60 minutes for Test 1, when concrete spalling occurred. For Test 2, the agreement at the top chord was within 10% for all locations except at location I, where the disagreement was substantial. The cause of this disagreement is not clear but it could possibly be attributed to the fact that the bridging truss acted as a thermal sink and that it was not included in the model.

Measured steel temperatures during fire tests indicated that the variation in temperatures among top chord, web diagonal, and bottom chord members was substantial. Also, there was large temperature variation along the length of the steel truss, which varied as tests progressed. These observations suggest that both initial conditions (variations in composition and geometry) and time varying boundary conditions (including the handling of material loss/transformation) are necessary to consider in order to predict the temporal and spatial variations of steel temperatures.

The present study provided the following information:

- A brief statistical evaluation of the thermal data recorded during the two full scale fire tests
- A practical approach for computing average temperatures at several positions along the main trusses (where measured temperature data were available) and a quantitative evaluation of the thermal model.
- A quantitative assessment of the agreement between the numerical and experimental results at several times into the tests.

For both tests, the modeled temperatures at the lower chord level were higher than the measured temperatures for most locations suggesting that error is systematic; however, at

both the top chord and mid-web level the deviation of measured temperatures from the ANSYS temperatures were not systematic. This indicates that the concrete slab (along with its variability of thermal properties due to time varying moisture levels) possibly plays a strong role in influencing the thermal behavior of steel members near its proximity. Note that the effects of moisture on concrete thermophysical properties and moisture migration in concrete were not included in the model.

The apparent dislodgement of SFRM at the top chord was incorporated in the ANSYS heat transfer model. By varying the length and depth of SFRM that was dislodged at specific locations, an agreement between the numerical and measured temperatures was achieved at four locations on the upper chord along a main truss. Such analysis can provide approximate information about the effect of dislodgement of SFRM on steel temperatures and a quantitative estimate of the extent of SFRM dislodgement may be possible by comparing modeled and measured temperatures using a trial and error approach or conducting an optimization procedure with a proper objective function.

The variability of the recorded steel temperatures highlights the need for characterization of uncertainties in predicting temperature histories of structural elements exposed to a damaging fire. Sources of variability may be:

- Moisture level in the concrete slab
- Applied thickness of SFRM on steel truss elements
- Dislodgement of SFRM (extent and thickness)
- Presence (amount) of overspray
- Non-uniform heating as a result of variation in view factors as well as the effective radiative temperature and volume emittance.

The time-temperatures data predicted by the numerical model are used in a structural model to study the effects of fire on the mechanical behavior of composite floor systems. The numerical heat transfer model needs to be improved by incorporating the most accurate data for both geometric changes in fire and thermophysical properties and heat transfer parameters such that predicted results are within 10 $^{\circ}$C (approximately) of measured temperatures especially at temperatures exceeding 400 $^{\circ}$C . This is because mechanical properties of steel (e.g., Young's modulus, yield strength etc.) decrease sharply when temperatures exceed 400 $^{\circ}$C. Accurate predictions of the thermal field will enhance the fidelity of structural predictions.

Sensitivity studies need to be conducted to determine the most important factors contributing to the variability in recorded temperatures. Determining uncertainties in time-dependent temperature histories of structural members in fire is necessary for predicting structural behavior in fire with a certain level of confidence.

7 References

1. ANSYS Mechanical Release 12.1 (2011), ANSYS Inc., Southpointe, 275 Technology Drive, Canonsburg, PA.
2. NIST (National Institute of Standards and Technology) (2005), Federal Building and Fire Safety Investigation of the World Trade Center Disaster: Final Report on the Collapse of the World Trade Center Towers, NIST NCSTAR 1-6B, Gaithersburg, MD.
3. NIST (National Institute of Standards and Technology) (2005), Federal Building and Fire Safety Investigation of the World Trade Center Disaster: Final Report on the Collapse of the World Trade Center Towers, NIST NCSTAR 1-6, Gaithersburg, MD.
4. ASTM (1973), "Standard Test Methods for Fire Tests of Building Construction and Materials", ASTM E119-73, ASTM International, Conshohocken, PA.
5. L.G. Blevins and W.M. Pitts (1999), "Modeling of Bare and Aspirated Thermocouples in Compartment Fire", Fire Safety Journal. 33. 239-259.
6. S. Lamont, A.S. Usmani, and D.D. Drysdale (2011), "Heat Transfer Analysis of the Composite Slab in the Cardington Frame Fire Tests", Fire Safety Journal 36: 815-839.
7. NIST (National Institute of Standards and Technology) (2005), Federal Building and Fire Safety Investigation of the World Trade Center Disaster: Final Report on the Collapse of the World Trade Center Towers, NIST NCSTAR 1-6A, Gaithersburg, MD.
8. ECI (1994), Eurocode 1: Basis of Design and Design Actions on Structures, Part 2-2: Action on Structures Exposed to Fire, ENV 1991-2-2, European Committee for Standardization, Brussels, Belgium.
9. (a) EC1 (2002), Eurocode 1: Actions on Structures. ENV 1991, Part 1-2: General Actions - Actions on Structures Exposed to Fire, Brussels, European Committee for Standardization, Brussels, Belgium.

   (b) EC2 (2002), Eurocode 2: Design of Concrete Structures. ENV 1992, Part 1-2: General Rules - Structural Fire Design, European Committee for Standardization, Brussels, Belgium.

   (c) EC3 (2002), Eurocode 3: Design of Steel Structures. ENV 1993, Part 1-2: General Rules- Structural Fire Design, European Committee for Standardization, Brussels, Belgium.

8 Acknowledgment

The authors gratefully appreciate many helpful comments provided by Drs. T.P. McAllister, J.A. Main, W. Grosshandler, and F. Sadek.

Appendix A: Thermophysical properties

1. Steel

The thermophysical properties listed here have been taken from Ref. [7].

A. Density = 7856.2 kg/m^3

B. Specific heat

Temperature ^{0}C	Specific heat J/kg/K
27	435.3
52	452.1
77	467.2
102	481.1
127	493.9
152	505.8
177	516.4
202	526.7
227	536.3
252	545.5
277	554.8
302	563.8
327	573.2
352	582.8
377	592.9
402	603.7
427	615.5
452	628.4
477	642.3
502	657.7
527	674.5
552	692.9
577	713.6
602	736.5
627	761.2
652	788.4
677	818.1
702	850.8

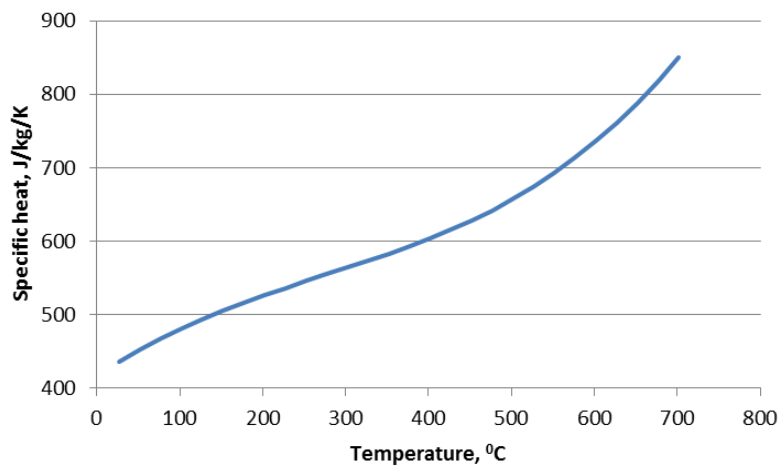

C. Thermal conductivity

Temperature ^0C	Thermal Conductivity W/m/K
27	47.6
52	47.8
77	47.8
102	47.6
127	47.2
152	46.8
177	46.2
202	45.5
227	44.8
252	44.1
277	43.3
302	42.5
327	41.7
352	40.8
377	40.0
402	39.2
427	38.3
452	37.5
477	36.7
502	35.9
527	35.1
552	34.3
577	33.5
602	32.8
627	32.0
652	31.3
677	30.6
702	30.0

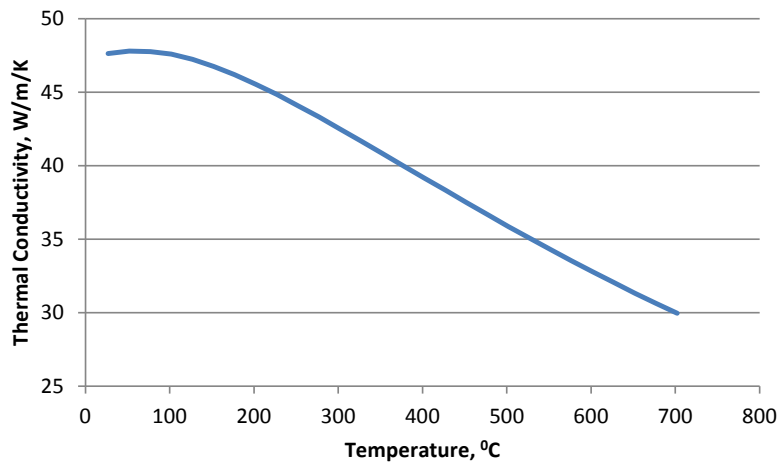

2. Concrete

A. Density

Temperature ^0C	Density kg/m3
23	2101.7
600	1951.5
800	1701.3
1000	1701.3

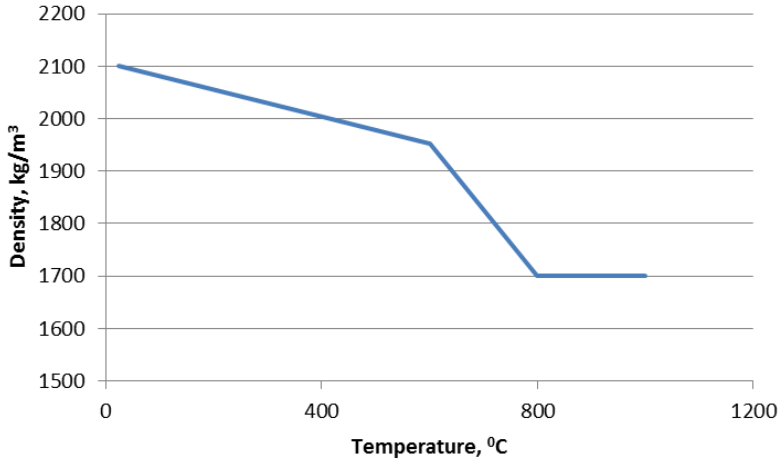

B. Specific heat

Temperature ^0C	Specific heat J/kg/K
23	900.6
100	1000.6
800	1000.6
810	1501.0
1000	1501.0

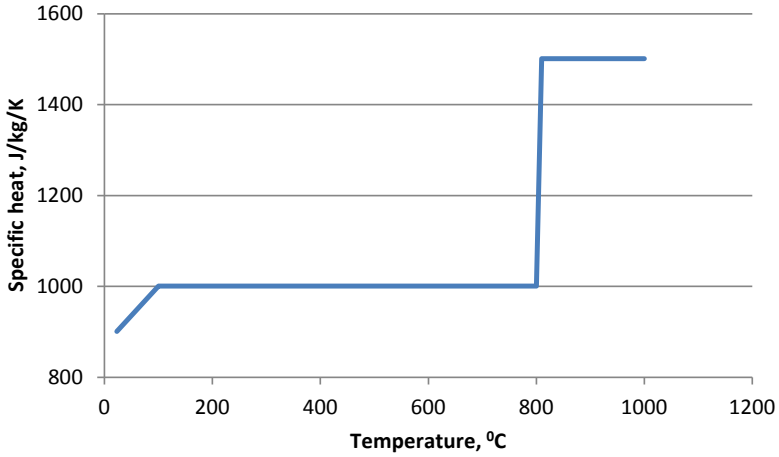

C. Thermal conductivity

Temperature ^0C	Thermal Conductivity W/m/K
23	1.5
800	1.0
1000	1.0

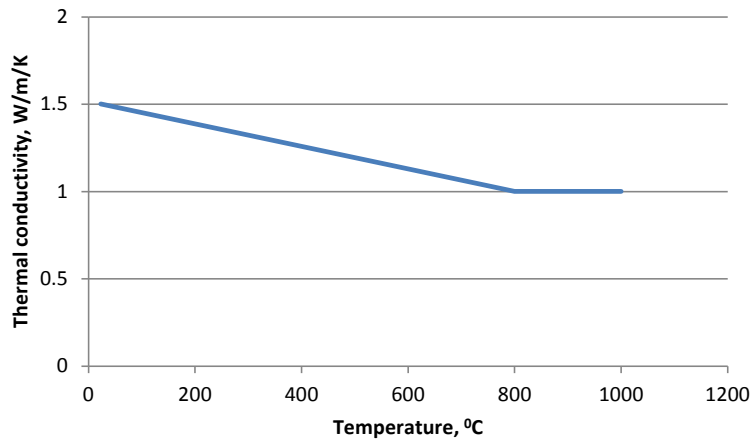

3. SFRM

A. Density

Temperature ^0C	Density kg/m^3
25	237.0
50	236.3
100	230.3
200	224.8
300	222.3
400	220.5
500	219.2
600	218.4
800	361.4
1000	376.1
1200	432.4

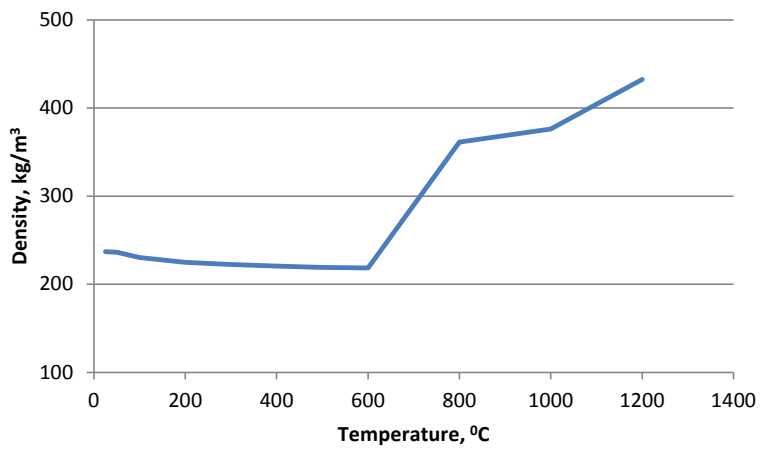

B. Specific heat

Temperature ^{0}C	Specific heat J/kg/K
25	826.9
50	942.0
100	724.3
200	897.6
300	1020.7
400	1071.4
500	1098.2
600	1190.3
800	1259.4
1000	1326.0
1200	1392.5

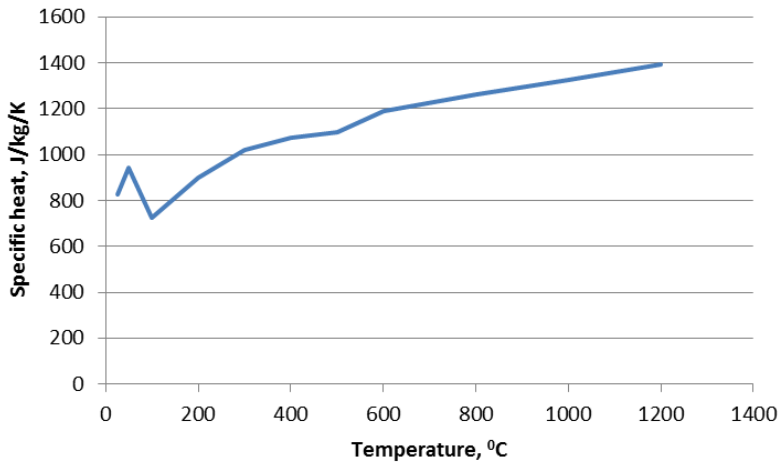

C. Thermal conductivity

Temperature ^{0}C	Thermal Conductivity W/m/K
25	0.0
50	0.1
100	0.1
200	0.1
300	0.1
400	0.1
500	0.2
600	0.2
800	0.3
1000	0.5
1200	0.5

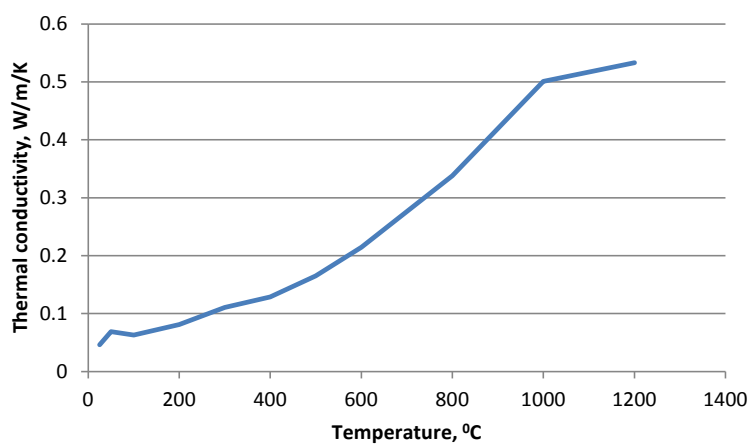

Appendix B: Finite Element Model of the Composite Floor System

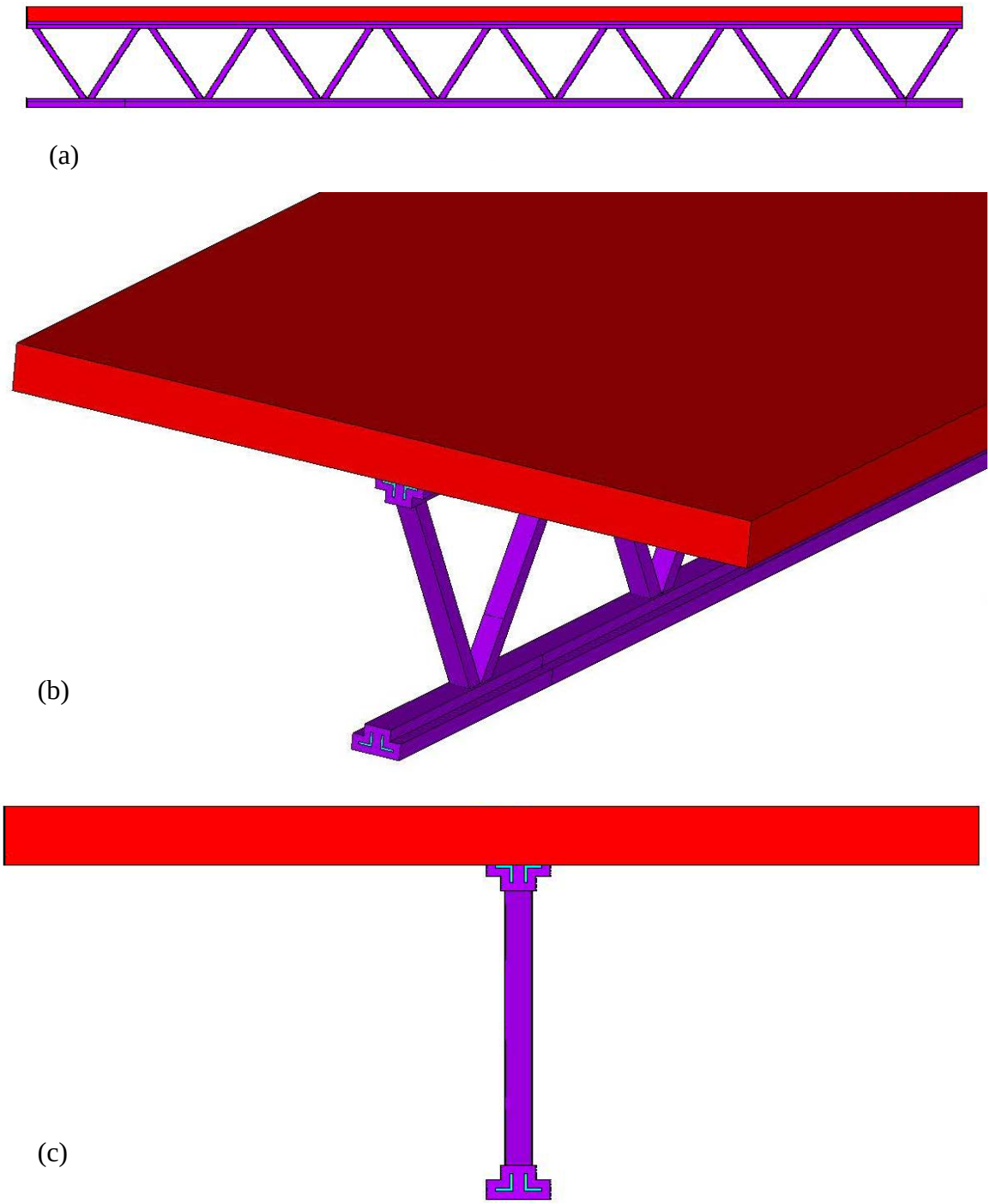

Figure B1: (a) side, (b) isometric, and (c) end-view of the FE model of the composite floor system.

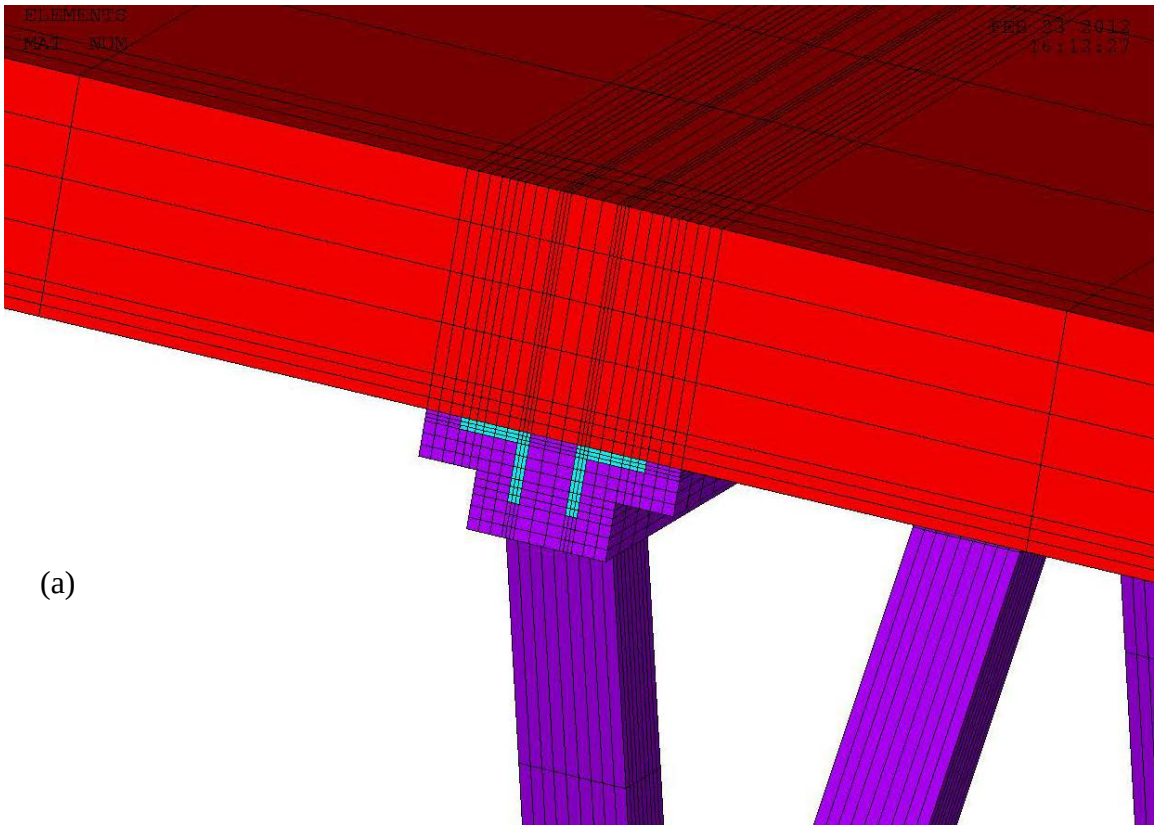

(a)

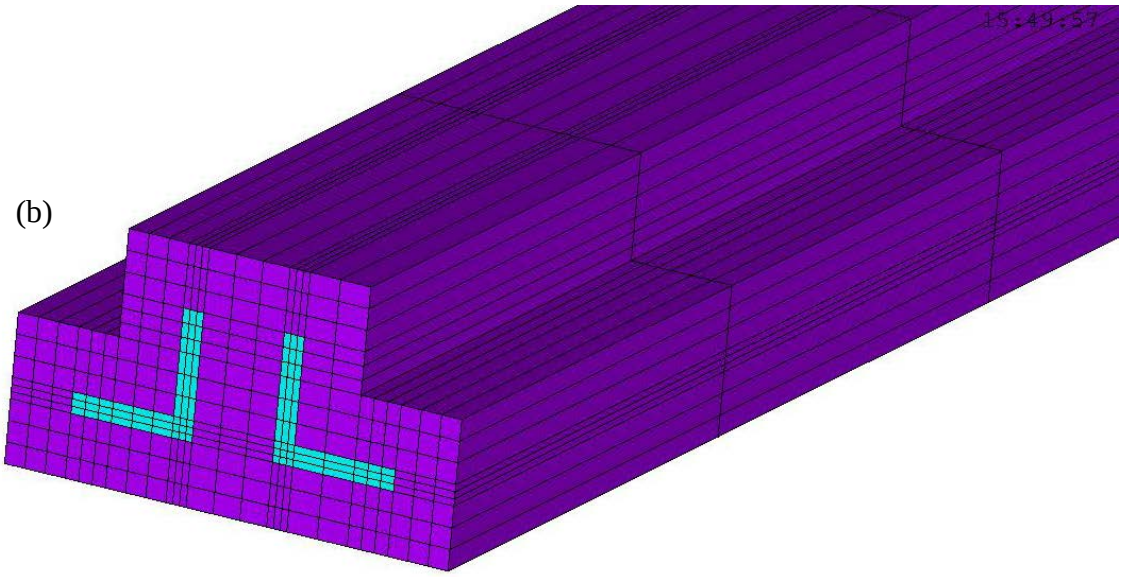

(b)

Figure B2: Discretization in the FEM model of the composite floor system: (a) upper chord and slab; (b) lower chord.

Appendix C: Log of Observations in Test 1

Test Time, Min	Exposed (E) or Unexposed (U) Surface	Observations
21	U	The concrete was spalling near the west end of the assembly.
23	E/U	Same observation as 21 minutes.
24	U	The concrete continued to spall.
25	E	Visual deflection was observed in the bottom chords of the bridging trusses.
26	E/U	Same observation as 21 minutes.
26	E	Visual deflection was observed on the deck spans between the trusses. Separation was observed in the deck seam above the center deck support angle.
27	E	The southeast metal deck seams began to separate.
29	E	Visual deflection was observed in the center deck support angle. The SFRM was turning brown in color.
33	E	The bridging trusses became more deformed. The vertical member on the west bridging truss where it intersects the south main truss was heavily deformed.
37	E	The deflection in the center deck support angle was more pronounced.
38	E/U	Reports heard.
44	E	The vertical members on all of the bridging trusses where they intersect the main trusses were deformed.
45	E	Large reports heard.
49	E/U	A loud report was heard near the center of assembly and a visible drop was observed.
53	E	One-half of the SFRM on the vertical member noted at 33 min. had fallen.
60	E	No additional fall off of SFRM on the bridging trusses.
63	E	The steel deck between west bridging truss and the deck support angle was 1/2 in. from the furnace thermocouple. The long diagonal web member on the south main truss was slightly bent.
68	E/U	Large report heard.
78	E/U	Large report heard.
78	E	The bottom chord of the north main truss, approximately 36 in. west of the assembly centerline, was deformed.
87	E	A 10 in. long piece of SFRM on the inner most angle of the lower chord on the north truss, 36 in west of the north-south centerline of the assembly fell.
88	E	A 7 to 10 in. long piece of SFRM on the inner most angle of the lower chord on the north truss, 36 in east of the north-south centerline of the assembly fell.
90	E	Additional SFRM at the area described at 87 min. peeling away but has not fallen.
92	E	A 12 in. long piece of sfrm on the inner most angle of the lower chord on the south truss, 36 in west of the north-south centerline of the assembly fell.
93	E	The area of fall off described at 87 min. had expanded to the three inner most angles.
109	E/U	A very large report was heard.
111	E/U	A very large report was heard.
116	E/U	Gas off, furnace fire extinguished.

Source: Reference [2]

Appendix D: Log of Observations in Test 2

Test Time, min	Exposed (E) or Unexposed (U) Surface	Observations
40	E & U	A large report was heard. Pronounced deck bow at the area noted in the 10 min. observation.
43	E	The web members of the bridging trusses began to deform.
46	E	The steel deck continued to deform.
48	E & U	Reports continued.
48.5	E & U	A report was heard.
50	E & U	A report was heard.
51.5	E & U	A report was heard.
53	E	Visual deflection of the center deck support angle was observed.
54	E & U	A report was heard.
56.5	E & U	A report was heard.
57	E & U	Three reports in a row were heard, approx. 1 second apart.
59.5	E & U	A report was heard.
60	E	All SFRM remained in place besides what was previously noted on the bridging trusses.
61	E & U	A report was heard.
63	E & U	A report was heard.
64	E & U	A report was heard.
72	E & U	A report was heard.
74	E	2 1/2 ft length of SFRM fell from the top angle of the east bridging truss.
75	E & U	A report was heard.
78	E & U	A report was heard.
84	E & U	A report was heard.
108	E	All SFRM remained on the main trusses.
120	E	All SFRM remained on the main trusses.
130	E & U	All observations were terminated due to safety precautions.
146	E & U	Gas off, fire test terminated.

Source: Reference [2]